IEEE Access
Multidisciplinary | Rapid Review | Open Access Journal

Received 28 July 2024, accepted 27 August 2024, date of publication 30 August 2024, date of current version 10 September 2024.

Digital Object Identifier 10.1109/ACCESS.2024.3452504

RESEARCH ARTICLE

Distributed Collaborative Optimization of Integrated Transportation-Power Energy Systems Considering Dynamic Wireless Charging

LIJUN GENG[1], CHENGXIA SUN[1], DONGDONG SONG[1], SHUANGHAN YANG[1], YUQUAN MA[1], AND ZHIGANG LU[2]

[1]Mechanical and Electrical Engineering College, Hebei Normal University of Science and Technology, Qinhuangdao 066004, China
[2]Key Laboratory of Power Electronics for Energy Conservation and Motor Drive of Hebei Province, Institute of Electrical Engineering, Yanshan University, Qinhuangdao 066004, China

Corresponding author: Lijun Geng (Li_jungeng@163.com)

This work was supported by the Doctoral Science Research Initiation Foundation of Hebei Normal University of Science and Technology under Grant 2023YB021.

ABSTRACT With the rapid advancement of transportation electrification, especially dynamic wireless charging technology, the interconnection between the transportation network and the power distribution network has become increasingly evident at both the informational and physical levels. Consequently, the emergence of integrated transportation-power energy systems has garnered considerable attention. It is urgent to realize a coordinated operation of the energy systems. In this paper, considering the elastic charging behavior and mileage limitation of electric vehicles, a modeling framework and corresponding solution algorithms are proposed to coordinate transportation and power distribution networks operation. In the transportation network, a traffic assignment model with the elastic charging demand and effective path generation models with the mileage limitation of electric vehicles are established to calculate the actual charging demand of electric vehicles and traffic flow distribution. In the power distribution network, an optimal power flow model based on second-order cone relaxation is established to calculate the power flow distribution and scheduling plans of generators. And then, based on the idea of alternating direction multiplier method, a distributed coordinated operation method and solution algorithm for the integrated transportation-power energy systems are proposed. Finally, a case study is performed to verify the effectiveness of the proposed model and algorithm.

INDEX TERMS Coordinated operation, dynamic wireless charging, electric vehicles, power distribution network, transportation network.

I. INTRODUCTION

In the process of energy revolution, the transportation network (TN) as lifeblood of economy has become an integral part of energy network. However, its substantial energy consumption and carbon emissions pose significant challenges to the sustainability of economic development. In recent years, electric vehicles (EVs) have emerged as the predominant decarbonized mode of transportation due to their energy-saving and environmentally friendly attributes [1]. The market penetration of EVs is experiencing rapid growth, and the development of an electrified transportation system centered around EVs is progressing swiftly [2]. In this context, novel interactions have arisen between transportation and power distribution systems, resulting in intricate operational control of both systems [3]. For example, traffic congestion status and policies will affect the driving behavior of EVs, and the choices of charging time and location will significantly affect the spatio-temporal distribution of charging load, and further affect the operation status of the power distribution network (PDN). The electricity price will, in turn, impacts the travelling and charging plans of EVs,

The associate editor coordinating the review of this manuscript and approving it for publication was S. Ali Arefifar.

thereby influencing the distribution of traffic flow on the TN. Fortunately, challenges always coexist with opportunities [4]. If the influence of charging load on the PDN is included in the TN model when designing traffic control strategies, it may have the potential to enhance the power flow distribution, operational safety, and economic efficiency of the PDN. Simultaneously, by considering the traffic characteristics of EVs in the scheduling plans of PDN, the adaptability of scheduling strategies can be enhanced and traffic congestion may be alleviated. Therefore, the research topic of cooperative optimization in power-transportation coupled networks emerges as an imperative and evolves into a novel interdisciplinary field of study [5].

Currently, there exist relevant literatures that have investigated the coordinated operation of the integrated transportation-power energy systems (ITPES) with the background of fast charging stations [6]. For example, the charging and driving paths of EVs in [7] are effectively regulated through the implementation of road congestion fees and electricity prices, thereby optimizing power flow efficiency and minimizing traffic travelling time. In [8], a holistic modeling framework is proposed to study the intertwined traffic and power flows in the ITPES. It is revealed that the coupled network will reach an equilibrium state, which is characterized by a fixed-point problem. Considering the elastic travel demand of EVs, a smart charging management system is designed in [9]. From the perspective of global decision maker, a cooperative pricing strategy for power-transportation coupled networks is proposed in [10] with the goal of optimal system operation. In [11], an optimal recovery strategy for coupled systems in the event of component failures is investigated. In [12], a generalized user equilibrium (GUE) method is proposed in the coordinated operation of ITPES to include the impact of PDN operation on the traffic equilibrium state. In [13], an N-1 security-constrained optimal traffic-power flow model is proposed to coordinate the ITPES toward N-1 secure and reliable.

Compared to plug-in charging, dynamic wireless charging offers a solution for EVs to charge while driving, eliminating the waiting time associated with traditional charging methods and enhancing the convenience of recharging [14]. Benefiting from its unique charging method, dynamic wireless charging has been extensively studied and demonstrated in engineering internationally. The broad implementation of in-motion EV-charging projects is expected in the near future [15]. In dynamic wireless charging mode, the coupling between TNs and PDNs becomes more tightly integrated as the coupling point shifts from static charging stations to mobile EVs, which instead enhances the engagement and timeliness of interaction between EV users and the power grid.

The research topic of collaborative optimization in ITPES under dynamic wireless charging mode has attracted widespread attention from scholars around the world. For example, to determine the optimal prices of electricity and roads to maximize social welfare, first-best and second-best pricing models are proposed under different authoritarian regimes in [16]. Reference [17] presents the short-term operation of dynamic wireless charging by capturing the interdependence among the electricity and transportation networks. The independent system operator, a public entity as mentioned in [18], is authorized to manage generation assets and impose congestion tolls on electrified roads with the objective of minimizing social costs. Subsequently, an optimal traffic-power flow model is proposed to determine the optimal generation schedule and congestion toll charges. Based on the [18], a multi-period optimal power and semi-dynamic traffic flow model is proposed in [19] considering the flow propagation between adjacent time periods. Under the dynamic wireless charging mode, EVs charging demand is shifted from residential plug-in charging to charging-while-driving during commuting hours, resulting in a simultaneous congestion in coupled networks. Consequently, a bi-level integrated demand response framework is further proposed in [20] to alleviate congestion in the ITPES. To accurately depict the time-varying electricity and traffic demands, the dynamic spatio-temporal coupling model of ITPES is established in [21] to simulate the spatio-temporal distribution of EV charging load and congestion cost. Different from the above studies that disregard the uncertainty of traffic demand and stochastic routing behavior of travelers, a robust dispatch method for the ITPES is proposed in [22] considering the PDN load perturbation caused by the traffic demand uncertainty, and an optimization modeling approach is presented in [23] based on hybrid stochastic user equilibrium/information gap decision theory method for coordinated operation of ITPES.

A detailed comparison of above mentioned literatures in the context of DWC is summarized in Table 1, from which we can identify the following inadequacies:

1) The state of charge (SOC) and range limitations of EVs during driving are ignored. Most existing studies often oversimplifies the modeling of TN by assuming that all EVs have identical energy demands and can reach any charging station within the TN, thereby disregarding crucial factors such as driving range limitations and battery state information. In reality, charging price and current SOC are crucial factors affecting recharging behavior of EVs during driving. For instance, when selecting a charging path, EV drivers must ensure that the battery does not deplete. Additionally, due to the impact of charging benefits, EV drivers may not fully recharge the battery while driving. EVs on different routes between different OD pairs will be influenced by charging prices and SOC, leading to different energy demands when passing through charging stations (roads).
2) The elasticity effect of EVs with rigid charging demand on travelling costs is not considered and modeled. The aforementioned literatures assume a fixed number of EVs that require charging during travel from origin to destination, without taking into account elastic responsive behavior of EV drivers to travelling costs.

TABLE 1. Comparison of relevant literatures related to dynamic wireless charging.

References	Traffic flow model	Power flow model	Regulation method	Solution method	Data privacy of TN and PDN	EVs' elasticity	EVs' mileage limitation and SOC
[16]	SO	DCOPF	Traffic toll, Electricity price	Manifold optimization algorithm	×	×	×
[17]	UE	DCOPF	Electricity price	Decentralized optimization	√	×	√
[18]	UE	ACOPF	Traffic toll	Mixed integer second-order cone program	×	×	×
[19]	Semi-dynamic UE	ACOPF	Traffic toll	Mixed integer second-order cone program	×	√	×
[20]	Multi-period UE	ACOPF	Traffic toll, Electricity price	A sequence of relaxed non-linear program	×	√	×
[21]	Dynamic UE	ACOPF	Electricity price	Fixed-Point Algorithms; Joint optimization algorithm	×	×	×
[22]	UE	ACOPF	Traffic toll	Two-stage robust second-order cone program	×	×	×
[23]	Stochastic UE	ACOPF	Traffic toll	SUE/IGDT optimization method	×	×	×
This Paper	Mixed UE	ACOPF	Electricity price	Adaptive path generation and solution algorithm; Distributed coordinated operation method	√	√	√

SO: Wardrop social optimal; UE: Wardrop user equilibrium; DCOPF: direct current optimal power flow; ACOPF: alternating current optimal power flow.

But in situations where the charging prices (costs) are excessively high or the driving distance is extensive, certain EVs may choose for alternative modes of transportation or even refrain from traveling altogether, deviating from their initial travelling and recharging plans.

3) Given the above two gaps, there still lacks a more detailed models of TN and an effective coordinated operation method and corresponding solution algorithms for ITPES in response to the elastic charging behavior and mileage limitation of EVs. How to maximize the social profit by tapping the flexibility of both elastic charging and energy demands of EVs while respecting PDN security constraints is still an open question.

In consideration of the above premises, this paper develops a modeling framework and corresponding solution algorithms considering the elastic charging behavior and mileage limitation of EVs to coordinate TNs and PDNs operation. The major contributions of this paper are summarized as follows:

1) A more detailed electrified TN model is established to accurately represent the SOC and mileage limitation of EVs during driving, as well as the elastic responsive behavior exhibited by EV drivers. In particular, an adaptive path generation and solution algorithm in TN is designed to iteratively determine the actual charging demand of EVs and traffic flow distribution.
2) In order to promote the coordinated operation of TNs and PDNs while ensuring data privacy between the two networks, the idea of alternating direction multiplier method (ADMM) is adopted to design a distributed coordinated operation method and solution algorithm for ITPES.
3) Numerical results on test system verify that the proposed detailed models of the TN, adaptive path generation and solution algorithm and distributed coordinated operation method of ITPES. In addition, we investigate the impacts of EVs penetration rate on the coordinated operation of TNs and PDNs.

II. MODEL FORMULATION

A. MODELING OF THE TRANSPORTATION NETWORK

The TN comprises two types of vehicles: some of them are EVs which need battery recharge, and others are traditional gasoline vehicles (GVs) along with EVs which do not need battery recharge. Specifically, the refueling behavior of GVs is neglected to simplify model and analysis, because it does not directly impact the PDN [8]. And EVs which do not need battery recharge, we treat them as traditional GVs and also call them GVs for simplicity, because they share a common route selection criterion with GVs. When traveling to their destinations, a GV seeks the route which has minimal travel time, and an EV looks for the route which minimizes its travel expense (cost) composed of the travel time and charging cost. And the origin-destination (OD) demands of GVs are fixed and known while EVs have elasticity in making charging and travelling plans. Keep those promises in mind, a traffic assignment model with the elastic charging demand and two types of effective path generation model are established to calculate actual charging demand of EVs and traffic flow distribution of TN.

1) ELASTIC BEHAVIOR MODEL

To depict the elastic behavior of EV drivers to travelling costs, an elastic demand function $q_{\mathrm{EV},\mathrm{real},w} = D_w(\mu_{\mathrm{EV},w})$ is introduced to calculate the actual charging demands after EVs response. This demand function is required to have the following two basic properties:

Property 1: the elastic demand function should be a continuously decreasing function of the minimum travelling

expense $\mu_{\mathrm{EV},w}$. This design is rooted in the dynamics of the TN, where the charging demand of EVs for each OD pair decreases with respect to the increase of minimum travelling expense.

Property 2: the elastic demand function must be strictly positive and possess an inverse function $D_w^{-1}(q_{\mathrm{EV},w})$. This inverse function serves as a representation of the utility level for EV users, demonstrating an escalation in value concomitant with the rise in charging demand for EVs.

Aligned with the aforementioned properties, we employ the widely acknowledged negative exponential function [24], [25] to describe the elastic demand of EVs, delineated by (1):

$$q_{\mathrm{EV,real},w} = D_w\left(\mu_{\mathrm{EV},w}\right) = q_{\mathrm{EV},w}\exp\left(-\theta\mu_{\mathrm{EV},w}\right) \quad (1)$$

where $q_{\mathrm{EV},w}$ and $q_{\mathrm{EV,real},w}$ represent the initial charging demand of EVs and the actual charging demand after EVs elastic response in OD pair w, respectively. θ is the elasticity coefficient, which represents degree of elastic responsiveness of EV users to the minimum travelling expense $\mu_{\mathrm{EV},w}$. The more pronounced the inclination of EVs to travel and recharge, the smaller the elasticity coefficient becomes.

2) TRAVELLING TIME AND TRAVELLING COST MODEL

Total path travelling time and travelling cost are the major consideration for road travelers to choose a route, and it depends on the congestion level of each road on the route. The road congestion level is usually quantified by a latency function $\chi_a(\psi_a)$ related to road flow ψ_a, which represents the actual travelling time of the road a. In practical TNs, the more vehicles a road carries, the longer the time required to traverse that road. Therefore, the latency function $\chi_a(\psi_a)$ is a strictly increasing function of road traffic flow ψ_a. Based on research findings from the Bureau of Public Roads (BPR) in the United States, it is often represented by the following BPR function [26].

$$\chi_a(\psi_a) = \chi_a^0\left[1 + b_a\left(\frac{\psi_a}{C_a}\right)^{\nu}\right], \quad \forall a \in \Omega_{\mathrm{A}} \quad (2)$$

where χ_a^0 equals the length of road a divided by speed limit, called the free-flow travelling time. Notation C_a denote the road capacity. The symbol b_a and ν are parameters of BPR function model, conventionally set at 0.15 and 4, respectively. The symbol Ω_{A} denotes the set of all roads in TN.

Every path comprises a set of roads, and this association can be delineated through the utilization of an indicator variable. If a path encompasses a particular road, the indicator variable $x_{a,kg,w}/x_{a,ke,w}$ is set to 1; otherwise, it is set to 0. It is noteworthy that this variable is predetermined and provided in advance based on the effective paths. Based on the road travelling time $\chi_a(\psi_a)$, the travelling time $\tau_{kg,w}$ and travelling cost $\zeta_{\mathrm{GV},kg,w}$ of each effective path kg for GVs between each OD pair w is able to be calculated by (3) and (4):

$$\tau_{kg,w} = \sum_{a=1}^{N_{\Omega_{\mathrm{A}}}} \chi_a(\psi_a)x_{a,kg,w} \ \forall kg \in \Omega_{\mathrm{KGV},w}, w \in \Omega_{\mathrm{OD}} \quad (3)$$

$$\zeta_{\mathrm{GV},kg,w} = \sum_{a=1}^{N_{\Omega_{\mathrm{A}}}} \eta\chi_a(\psi_a)x_{a,kg,w} \ \forall kg \in \Omega_{\mathrm{KGV},w}, w \in \Omega_{\mathrm{OD}} \quad (4)$$

where η signifies the conversion coefficient for time and cost, with a nominal value of \$10/h. The symbol $\Omega_{\mathrm{KGV},w}$ and Ω_{OD} denote set of effective paths for GVs and the set of all travel OD pairs in TN, respectively.

Similarly, the travelling time $\tau_{ke,w}$ of each effective path ke for EVs between each OD pair w can be calculated by (5):

$$\tau_{ke,w} = \sum_{a=1}^{N_{\Omega_{\mathrm{A}}}} \chi_a(\psi_a)x_{a,ke,w} \ \forall ke \in \Omega_{\mathrm{KEV},w}, w \in \Omega_{\mathrm{OD}} \quad (5)$$

where symbol $\Omega_{\mathrm{KGV},w}$ denotes set of effective paths for EVs.

Diverging from travelling cost of GVs, the travelling cost $\zeta_{\mathrm{EV},ke,w}$ for an EV driver experienced on the effective path ke becomes the summation of travelling time cost and charging cost, which is given by:

$$\zeta_{\mathrm{EV},ke,w} = \sum_{a=1}^{N_{\Omega_{\mathrm{A}}}} \eta\chi_a(\psi_a)x_{a,ke,w} + \sum_{a=1}^{N_{\Omega_{\mathrm{A}}}} \lambda_{a\in s\in j}E_{a,ke,w} \quad \forall ke \in \Omega_{\mathrm{KEV}}, w \in \Omega_{\mathrm{OD}} \quad (6)$$

where $\lambda_{a\in s\in j}$ denotes charging electricity price of road a, namely the node marginal electricity price of PDN bus j, which provides power to the dynamic wireless charging station s. Simultaneously, $E_{a,ke,w}$ stands for the charging quantity when the effective path ke between the OD pair w traverses road a, it is optimized by the subsequently proposed effective path generation model for EVs.

3) TRAFFIC FLOW MODEL

To ensure traffic flow conservation, the total traffic flow for each travel OD pair should equal the sum of traffic flows on all effective paths for that OD pair.

$$\sum_{kg=1}^{N_{\Omega_{\mathrm{KGV},w}}} H_{\mathrm{GV},kg,w} = q_{\mathrm{GV},w} \ \forall w \in \Omega_{\mathrm{OD}} \quad (7)$$

$$\sum_{ke=1}^{N_{\Omega_{\mathrm{KEV},w}}} H_{\mathrm{EV},ke,w} = q_{\mathrm{EV,real},w} \ \forall w \in \Omega_{\mathrm{OD}} \quad (8)$$

where $H_{\mathrm{GV},kg,w}(H_{\mathrm{EV},ke,w})$ represents traffic flow of GVs (EVs) on effective path $kg(ke)$ between travel OD pair w. $q_{\mathrm{GV},w}$ is the traffic demand of GVs between the travel OD pair w.

Similarly, adhering to the traffic conservation theorem, the total traffic flow ψ_a on any road a is equal to the sum of the traffic flows of all effective paths for GVs and EVs that will pass through road a, which can be presented by (9)-(11).

$$\psi_a = \psi_{\mathrm{EV},a} + \psi_{\mathrm{GV},a} \ \forall a \in \Omega_{\mathrm{A}} \quad (9)$$

$$\psi_{\mathrm{GV},a} = \sum_{w=1}^{N_{\Omega_{\mathrm{OD}}}} \sum_{kg=1}^{N_{\Omega_{\mathrm{KGV},w}}} H_{\mathrm{GV},kg,w}x_{a,kg,w} \ \forall a \in \Omega_{\mathrm{A}} \quad (10)$$

$$\psi_{\mathrm{EV},a} = \sum_{w=1}^{N_{\Omega_{\mathrm{OD}}}} \sum_{ke=1}^{N_{\Omega_{\mathrm{KEV},w}}} H_{\mathrm{EV},ke,w} x_{a,ke,w} \ \forall a \in \Omega_{\mathrm{A}} \tag{11}$$

Additionally, the path flows for GVs and EVs must adhere to the non-negativity constraints outlined in (12) and (13):

$$H_{\mathrm{GV},kg,w} \geq 0 \ \forall kg \in \Omega_{\mathrm{KGV},w}, w \in \Omega_{\mathrm{OD}} \tag{12}$$

$$H_{\mathrm{EV},ke,w} \geq 0 \ \forall ke \in \Omega_{\mathrm{KEV},w}, w \in \Omega_{\mathrm{OD}} \tag{13}$$

4) MIXED USER EQUILIBRIUM CONDITIONS

In the actual TNs, traffic users consistently tend to favor paths with minimal travelling costs. Influenced by the traffic congestion effects, there exists an interactive influence between the path selections of EVs and GVs. This interplay among vehicles ultimately leads to the attainment of a stable state in the electrified TN, known as the User Equilibrium (UE) [27], [28]. In this equilibrium state, each traveler is unable to reduce their travelling costs by adjusting their route choice. In other words, when the electrified TN reaches this equilibrium state, every utilized path kg/ke for each travel OD pair possesses equal and minimal travelling expense $\mu_{\mathrm{GV},w}$/$\mu_{\mathrm{EV},w}$, while the travelling costs for paths not be chosen exceed this minimum travelling expense.

This equilibrium state can be mathematically interpreted as the following complementarity constraints.

$$0 \leq H_{\mathrm{GV},kg,w} \perp \zeta_{\mathrm{GV},kg,w} - \mu_{\mathrm{GV},w} \geq 0 \quad \forall kg \in \Omega_{\mathrm{KGV},w}, w \in \Omega_{\mathrm{OD}} \tag{14}$$

$$0 \leq H_{\mathrm{EV},ke,w} \perp \zeta_{\mathrm{EV},ke,w} - \mu_{\mathrm{EV},w} \geq 0 \quad \forall ke \in \Omega_{\mathrm{KEV},w}, w \in \Omega_{\mathrm{OD}} \tag{15}$$

where $0 \leq a \perp b \geq 0$ stands for $a \geq 0$, $b \geq 0$ and $ab = 0$.

5) TRAFFIC ASSIGNMENT MODEL WITH ELASTIC CHARGING DEMAND

To sum up, Equations (1)-(15) constitute a traffic assignment model with elastic charging demand. However, the complementary constraints illustrated in (14)-(15) violate the restrictions of standard constraints. This nonlinear comple-mentary constraint form makes it challenging to solve the traffic assignment model using general nonlinear solvers. Following paradigm in [29], it turns out that Equations (1)-(15) can be used to constitute the Karush–Kuhn–Tucker (KKT) conditions of following strictly convex optimization problem with linear constraints, which is called a traffic assignment problem with elastic charging demand (TAP-ECD):

$$\begin{aligned} &\min F_{\mathrm{TAP}} = F_{\mathrm{T}} + F_{\mathrm{CH}} - \mathrm{U_E} \\ &\text{s.t. } \{(7) - (13)\} \end{aligned} \tag{16}$$

Thus, the traffic assignment model with elastic charging demand can be equivalent calculated by this optimization problem (16). The objective function consists of three components: the first term is the total traffic delay cost F_T associated with travelling time of road a; the second term is the total charging cost F_{CH} for all of the EVs; the third term is the total utility for EVs participating in elastic response.

$$\begin{aligned} F_{\mathrm{T}} &= \sum_{a=1}^{N_{\Omega_{\mathrm{A}}}} \eta \int_0^{\psi_a} \chi_a(\psi_a)\, \mathrm{d}\psi_a \\ &= \sum_{a=1}^{N_{\Omega_{\mathrm{A}}}} \eta \chi_a^0 \left[\psi_a + \frac{b_a(\psi_a)^{\nu+1}}{\nu(C_a)^{\nu}} \right] \end{aligned} \tag{17}$$

$$\begin{aligned} F_{\mathrm{CH}} &= \sum_{w=1}^{N_{\Omega_{\mathrm{OD}}}} \sum_{ke=1}^{N_{\Omega_{\mathrm{KEV},w}}} \int_0^{H_{\mathrm{EV},ke,w}} \sum_{a=1}^{N_{\Omega_{\mathrm{A}}}} \lambda_{a \in s \in j} E_{a,ke,w} \mathrm{d}H_{\mathrm{EV},ke,w} \\ &= \sum_{w=1}^{N_{\Omega_{\mathrm{OD}}}} \sum_{ke=1}^{N_{\Omega_{\mathrm{KEV},w}}} \left(\sum_{a=1}^{N_{\Omega_{\mathrm{A}}}} \lambda_{a \in s \in j} E_{a,ke,w} \right) H_{\mathrm{EV},ke,w} \end{aligned} \tag{18}$$

$$\begin{aligned} \mathrm{U_E} &= \sum_{w=1}^{N_{\Omega_{\mathrm{OD}}}} \int_0^{q_{\mathrm{EV,real},w}} D_w^{-1}(y) \mathrm{d}y \\ &= \sum_{w=1}^{N_{\Omega_{\mathrm{OD}}}} \int_0^{q_{\mathrm{EV,real},w}} \frac{1}{\theta} \ln(q_{\mathrm{EV},w}) - \ln(q_{\mathrm{EV,real},w}) \mathrm{d}y \\ &= \frac{1}{\theta} \sum_{w=1}^{N_{\Omega_{\mathrm{OD}}}} \left[\ln(q_{\mathrm{EV},w}) - \ln(q_{\mathrm{EV,real},w}) + 1 \right] q_{\mathrm{EV,real},w} \end{aligned} \tag{19}$$

Therefore, the above TAP-ECD is strictly convex optimization problem with linear constraints, and can be efficiently solved by nonlinear solvers such as IPOPT.

6) EFFECTIVE PATH GENERATION MODEL

In previous studies [16], [17], [18], [19], [20], [21], [22], [23], the sets of travelling paths for EVs and GVs between each OD pair involved in TAP-ECD, denoted as Ω_{KEV} and Ω_{KGV}, respectively, can be enumerated offline through path search algorithms. However, due to the inherent tendency of drivers to choose the paths with the minimum travelling expense during their journeys, the majority of enumerated feasible paths are unlikely to be selected by drivers resulting in redundant paths, which significantly escalate the computational complexity of the TAP-ECD. Moreover, the route choices for EVs, unlike GVs, are influenced not only by travelling distance limitations but also by charging decisions including selection of charging roads and charging electricity quantities. If an enumeration method is still employed for the analysis of EVs paths, the computational burden would be exceedingly substantial, potentially rendering it impractical. Therefore, considering the travelling distance limitations and battery status for EVs, we propose effective path generation models to construct the effective path sets Ω_{KEV} and Ω_{KGV} for both EVs and GVs.

The fundamental idea behind the effective path generation model is to optimize for the maximum travelling benefit for EVs (minimum travelling cost for GVs) between each OD pair under the current traffic flow distribution, resulting in the selection of an optimal travel path $\upsilon_{ke}(\upsilon_{kg})$.

1) Effective path generation model for EVs

Influenced by charging preferences of drivers, EVs may not be fully replenish energy during driving. EVs on different travelling paths between distinct OD pairs may exhibit varying energy demands when passing through charging roads, which are affected by charging electricity prices and battery states. Therefore, the effective path generation model for EVs (EPM-EVs) is not only required to determine an appropriate travel path but also optimize the charging electricity quantity of the charging road along that path based on the battery status of EVs.

To describe the charging behavior of replenishing energy for EVs during the travel process, the concept of utility functions from microeconomics is adopted for analysis and modeling. In actual TNs, EV drivers who choose the same driving path often exhibit similar charging behavior, so the utility function $\mathrm{U}_{\mathrm{EV},ke,w}$ for EV drivers on each path ke between each OD pair w can be unified. This utility function is required to have the following two basic properties:

Property 1: the charging utility function $\mathrm{U}_{\mathrm{EV},ke,w}(E_{a,ke,w}, \omega)$ for EV drivers should be a non-decreasing function of the charging electricity quantity $E_{a,ke,w}$. Because drivers tend to replenish energy as much as possible until reaching the permissible maximum charging capacity, it can be asserted that user satisfaction and utility levels progressively increase with the augmentation of charging electricity quantity. When the charging electricity quantity of the EV attains the maximum value M, users charging satisfaction reaches its peak, conforming to the functional characteristic expressed in (20):

$$\frac{\partial \mathrm{U}_{\mathrm{EV},ke,w}(E_{a,ke,w}, \omega)}{\partial E_{a,ke,w}} \geq 0, \quad 0 \leq E_{a,ke,w} \leq M \tag{20}$$

where symbol ω is a parameter of charging utility function. It reflects the sensitivity of driver to charging electricity price. The larger the parameter value, the stronger the charging willingness of EV drivers to fully recharge the battery. Next, the partial derivative of the charging utility function to the charging electricity quantity, Equation (20), is further defined as the charging marginal revenue $V_{\mathrm{EV},ke,w}(E_{\mathrm{EV},ke,w}, \omega)$ of EV drivers, which is expressed by (21):

$$V_{\mathrm{EV},ke,w}(E_{\mathrm{EV},ke,w}, \omega) = \frac{\partial U_{\mathrm{EV},ke,w}(E_{\mathrm{EV},ke,w}, \omega)}{\partial E_{\mathrm{EV},ke,w}}, \quad 0 \leq E_{\mathrm{EV},ke,w} \leq M \tag{21}$$

Property 2: the charging marginal revenue $V_{\mathrm{EV},ke,w}(E_{\mathrm{EV},ke,w}, \omega)$ of EV drivers should exhibit a non-increasing trend with respect to the charging electricity quantity $E_{a,ke,w}$. As the charging electricity quantity increases, the charging utility of EV drivers tends to reach saturation, resulting in a subsequent decline in their marginal revenue.

$$\frac{\partial V_{\mathrm{EV},ke,w}(E_{\mathrm{EV},ke,w}, \omega)}{\partial E_{\mathrm{EV},ke,w}} \leq 0 \tag{22}$$

There are many types of utility functions that satisfy both of these properties. Considering the charging characteristics of EVs, we employ the widely used piecewise quadratic function in [30] to quantify the charging utility of EV drivers traversing charging roads on each charging path between each OD pair. The specific model is presented in (23):

$$U_{\mathrm{EV},a,ke,w}(E_{a,ke,w}, \omega) = \begin{cases} E_{a,ke,w}(\omega - \frac{\alpha}{2}E_{a,ke,w}), & 0 \leq E_{a,ke,w} \leq \frac{\omega}{\alpha} \\ \frac{\omega^2}{2\alpha}, & E_{a,ke,w} \geq \frac{\omega}{\alpha} \end{cases} \tag{23}$$

where α is a preset parameter, which affects peak value of the utility function. When variable $E_{a,ke,w}$ maps to the peak value, charging road will output the maximum charging electricity quantity L_a it can provide, and then

$$\frac{\omega}{\alpha} = L_a, \quad \alpha = \frac{\omega}{L_a} \tag{24}$$

Combining with Equation (23) and Equation (24), the final charging utility function of EV drivers on the path ke between OD pair w is obtained, as shown in (25):

$$U_{\mathrm{EV},ke,w} = \sum_{a=1}^{N_{\Omega_\mathrm{A}}} \left[\omega E_{a,ke,w} - \frac{\omega}{2L_a}(E_{a,ke,w})^2 \right] \tag{25}$$

In effective path generation model for EVs, if only considering maximizing the charging utility or minimizing the travelling cost of EV drivers to obtain the optimal charging path and charging electricity quantity, it will not maximize the travelling benefit for EVs. Therefore, considering the driving range limitations and battery states of EVs, this paper establishes EPM-EVs with the goal of maximizing the travelling benefit $W_{\mathrm{EV},ke,w}$ of EVs, as shown in (26), (28)-(35).

Objective function:

$$\max_{\gamma,E} W_{\mathrm{EV},ke,w} = \mathrm{U}_{\mathrm{EV},ke,w} - \kappa_{\mathrm{EV},ke,w} \tag{26}$$

$$\kappa_{\mathrm{EV},ke,w} = \sum_{a=1}^{N_{\Omega_\mathrm{A}}} \left[\eta \chi_a(\psi_a) \gamma_{a,ke} + \lambda_{a \in s \in j} E_{a,ke,w} \right] \tag{27}$$

where $\kappa_{\mathrm{EV},ke,w}$ is travelling cost of EVs in path ke between OD pair w. $\gamma_{a,ke}$ is an 0-1 decision variable, and if the path ke includes road a, then $\gamma_{a,ke} = 1$, otherwise, $\gamma_{a,ke} = 0$.

Constraints:

$$\Delta\gamma_{ke,w} = \mathbf{I}_{\mathrm{EV},w} \ \forall w \in \Omega_{\mathrm{OD}} \tag{28}$$

$$\mathrm{SOC}_{i,ke,w} - d_a\varpi + E_{a,ke,w} - \mathrm{SOC}_{j,ke,w} = \varepsilon_{a,ke,w} \quad \forall (i,j) = a \in \Omega_\mathrm{A} \tag{29}$$

$$\begin{cases} \varepsilon_{a,ke} \geq -\mathrm{M}\left(1 - \gamma_{a,ke}\right) \\ \varepsilon_{a,ke} \leq \mathrm{M}\left(1 - \gamma_{a,ke}\right) \end{cases} \quad \forall (i,j) = a \in \Omega_\mathrm{A} \tag{30}$$

$$\mathrm{SOC}_{i,ke,w} - d_a\varpi + E_{a,ke,w} \geq -\mathrm{M}\left(1 - \gamma_{a,ke,w}\right) + m \quad \forall (i,j) = a \in \Omega_\mathrm{A} \tag{31}$$

$$\mathrm{SOC}_{i,ke,w} - d_a\varpi + E_{a,ke,w}$$

$$\leq \mathrm{M}\left(1-\gamma_{a,ke,w}\right)+\mathrm{SOC}_{\max}\ \forall\,(i,j)=a\in\Omega_{\mathrm{A}} \tag{32}$$

$$\begin{cases} 0\leq E_{a,ke,w}\leq L_a\gamma_{a,ke,w} & \text{if } a\in c\in\Omega_{\mathrm{WCS}} \\ E_{a,ke,w}=0 & \text{if } a\notin c\in\Omega_{\mathrm{WCS}} \end{cases} \tag{33}$$

$$\mathrm{SOC}_{r,ke,w} = \mathrm{SOC}_{\mathrm{ini},w} \tag{34}$$

$$\mathrm{SOC}_{\mathrm{end},w} \leq \mathrm{SOC}_{s,ke,w}\leq \mathrm{SOC}_{\max} \tag{35}$$

Equation (28) constrains all possible paths between each OD Pair. The node-link incidence matrix Δ depicts the network topology. Each column of Δ corresponds to a road and has two non-zero elements: 1 (-1) at the component associated with the entrance (exit) node. In view of the definition of Δ, $\gamma_{ke,w}$ represents a chain of connected roads from origin r and travels to its destination s. $\mathbf{I}_{\mathrm{EV},w}$ has two non-zero elements, 1 and -1 at the entries corresponding to the origin node r and the destination node s. Equations (29) and (30) represent the battery charge variation experienced by an EV when traveling through any road. $\mathrm{SOC}_{i,ke,w}$ and $\mathrm{SOC}_{j,ke,w}$ represent the initial and final state of charge (SOC), respectively, for the EV when it travels through the road on a path ke between OD pair w. Notations d_a and ϖ denote the distance of road and driving energy consumption rate of EVs, respectively. The symbols $\varepsilon_{a,ke}$ and M are Auxiliary variable and infinite constant. Equations (31) and (32) take into account the impact of range limitations and battery capacity of EVs. When EV traverses a certain road and arrives at the next node, the SOC should not fall below a certain threshold m and not exceed the maximum capacity $\mathrm{SOC}_{\max}$. Equation (33) indicates that if the charging path taken by the EVs involves a dynamic wireless charging road, the charging electricity quantity $E_{a,ke,w}$ in that road is constrained to be less than the maximum charging quantity L_a; otherwise, the charging electricity quantity is set to zero. $\mathrm{SOC}_{r,ke,w}$ and $\mathrm{SOC}_{\mathrm{end},w}$ are the SOC of EV at the origin r and at the destination s, respectively.

1. Effective path generation model for GVs

The effective path generation model for GVs (EPM-GVs) is comparatively straightforward, as depicted in (36)-(37):

$$\min \kappa_{\mathrm{GV},kg,w}=\sum_{a=1}^{N_{\Omega_{\mathrm{A}}}}\eta\chi_a(\psi_a)\gamma_{a,kg} \tag{36}$$

$$\Delta\gamma_{kg}=I_{\mathrm{GV},w}\ \forall w\in\Omega_{\mathrm{OD}} \tag{37}$$

The above two effective path generation models are mixed integer linear programming problem and can be effectively solved using CPLEX or Mosek solvers.

7) ADAPTIVE PATH GENERATION AND SOLUTION ALGORITHM

Combining the TAP-ECD established in Section V) and two types of the effective path generation model developed in Section 6), an adaptive path generation and solution algorithm is designed specifically to calculate actual charging demand of EVs and traffic flow distribution of TN. The detailed algorithm process is illustrated in TABLE 2.

TABLE 2. Adaptive path generation and solution algorithm.

Algorithm 1: Adaptive Path Generation and Solution Algorithm

Input:

1: Road information and OD matrix for TN.

Initialization:

2: Set ψ_a=0, $\forall a\in\Omega_{\mathrm{A}}$.

3: For $w=1:N_{\Omega_{OD}}$ do

4: Solve the optimization problems EPM-EVs (26, 28-35) and EPM-GVs (36-37) under zero traffic flow to obtain initial effective paths υ_{ke} and υ_{kg}.

5: Build initial effective path sets Ω_{KEV} and Ω_{KGV}, set $\Omega_{\mathrm{KEV}}\leftarrow[\upsilon_{ke}]$ and $\Omega_{\mathrm{KGV}}\leftarrow[\upsilon_{kg}]$.

6: End for

Iterative program:

7: For $n=1:N_{\max}$ do

8: Solve the optimization problem TAP-ECD (16) with current effective path sets Ω_{KEV} and Ω_{KGV}, then, obtain the optimal traffic flow ψ_a^*, $\forall a\in\Omega_{\mathrm{A}}$.

9: Update travelling costs $\zeta_{\mathrm{EV},ke,w}$ and $\zeta_{\mathrm{GV},kg,w}$ for each path according to (4) and (6) with the obtained traffic flow ψ_a^*, $\forall a\in\Omega_{\mathrm{A}}$ in step 8.

10: Find minimal travelling expenses $\mu_{\mathrm{EV},w}$ and $\mu_{\mathrm{GV},w}$ between OD pair w.

11: Solve EPM-EVs (26, 28-35) and EPM-GVs (36-37) for each OD pair to obtain the new effective paths υ_{ke} and υ_{kg}, and calculate the corresponding travelling costs $\kappa_{\mathrm{EV},ke,w}$ and $\kappa_{\mathrm{GV},kg,w}$ using (27) and (36), respectively.

12: **Convergence Check:** If $\kappa_{\mathrm{EV},ke,w}\geq\mu_{\mathrm{EV},w}$, $\kappa_{\mathrm{GV},kg,w}\geq\mu_{\mathrm{GV},w}$, $\forall w\in\Omega_{\mathrm{OD}}$, terminate the iteration program, and go to step 15. Otherwise, if $\kappa_{\mathrm{EV},ke,w}<\mu_{\mathrm{EV},w}$, $\forall w\in\Omega_{\mathrm{OD}}$, then set $\Omega_{\mathrm{KEV},w}\leftarrow[\Omega_{\mathrm{KEV},w},\upsilon_{ke}]$; if $\kappa_{\mathrm{GV},kg,w}<\mu_{\mathrm{GV},w}$ $\forall w\in\Omega_{\mathrm{OD}}$, then set $\Omega_{\mathrm{KGV},w}\leftarrow[\Omega_{\mathrm{KGV},w},\upsilon_{kg}]$

13: Update effective path sets Ω_{KEV} and Ω_{KGV}, and go to step 7.

14: End for.

Output:

15: Effective path sets Ω_{KEV} and Ω_{KGV}.

16: Charging load of EVs.

17: Traffic flow distribution results of TN.

B. MODELING OF THE POWER DISTRIBUTION NETWORK

Power distribution system contains dynamic wireless charging stations (WCS) and generators which are connected to electric buses of PDN. The PDN is served by a typical radial network. Based on the characteristics, an optimal power flow model based on second-order cone relaxation (OPF-SOCR) [31] is formulated to calculate optimal power flow distribution and the scheduling plans of generators.

The objective of OPF-SOCR is to minimize operation cost F_{E} of PDN including the electricity purchasing cost F_{sub} from the wholesale power market as well as the production cost F_{G} of generators.

$$\min F_{\mathrm{E}}=F_{\mathrm{sub}}+F_{\mathrm{G}} \tag{38}$$

$$F_{\text{sub}} = \sum_{j=1}^{N_{\text{sub}}} \rho_{\text{sub}} P_{\text{sub},j} \tag{39}$$

$$F_{\text{G}} = \sum_{g=1}^{N_{\text{G}}} \left[a_g (P_{\text{G},g})^2 + b_g P_{\text{G},g} \right] \tag{40}$$

where ρ_{sub} represents the unit cost of purchasing electricity from the higher-level power grid. $P_{\text{sub},j}$ denotes active power delivered through line connected to the slack bus. $P_{\text{G},g}$ represents the active power of the generator. Notations a_g and b_g are production cost coefficients of generator.

The OPF-SOCR is subjected to branch flow equations proposed in [32] and [33] as shown in (41)-(45):

$$P_{i,j} + P_{\text{G},j} - I_{i,j} r_{i,j} = \sum_{h=1}^{N_j} P_{j,h} + P_{\text{L},j} \; \forall (i,j) \in \Omega_{\text{L}} \tag{41}$$

$$P_{\text{L},j} = P_{\text{Lc},s\in j} + P_{\text{Ld},j} \; \forall j \in \Omega_{\text{N}} \tag{42}$$

$$Q_{i,j} + Q_{\text{G},j} - I_{i,j} x_{i,j} = \sum_{h=1}^{N_j} Q_{j,h} + Q_{\text{L},j} \; \forall (i,j) \in \Omega_{\text{L}} \tag{43}$$

$$U_i - U_j = 2(r_{i,j} P_{i,j} + x_{i,j} Q_{i,j}) - [(r_{i,j})^2 + (x_{i,j})^2] I_{i,j} \forall (i,j) \in \Omega_{\text{L}} \tag{44}$$

$$I_{i,j} U_i \geq (P_{i,j})^2 + (Q_{i,j})^2 \; \forall (i,j) \in \Omega_{\text{L}} \tag{45}$$

where (45) denotes the SOC relaxation. $P_{i,j}$ and $Q_{i,j}$ are the active and reactive power of branch (i,j). $P_{j,h}$ and $Q_{j,h}$ are the active and reactive power of branch (j,h) connected to node j. $r_{i,j}$ and $x_{i,j}$ are the resistance and reactance of branch (i,j). $Q_{\text{G},g}$ represents the reactive power of the generator. $P_{\text{L},j}$ and $Q_{\text{L},j}$ are the active and reactive power demand at node j. $P_{\text{Lc},s\in j}$ and $P_{\text{Ld},j}$ are the charging and regular loads at node j. $I_{i,j}$ and U_j represent square of current magnitude in branch (i,j) and square of voltage magnitude at node j,respectively.

Furthermore, the security constraints of PDN are also considered as shown in (46)-(51):

$$(P_{i,j})^2 + (Q_{i,j})^2 \leq (S_{i,j}^{\max})^2 \; \forall (i,j) \in \Omega_{\text{L}} \tag{46}$$

$$P_{i,j} - r_{i,j} I_{i,j} \geq 0 \; \forall (i,j) \in \Omega_{\text{L}} \tag{47}$$

$$Q_{i,j} - x_{i,j} I_{i,j} \geq 0 \; \forall (i,j) \in \Omega_{\text{L}} \tag{48}$$

$$U_j^{\min} \leq U_j \leq U_j^{\max} \; \forall j \in \Omega_{\text{N}} \tag{49}$$

$$P_{\text{G},g}^{\min} \leq P_{\text{G},g} \leq P_{\text{G},g}^{\max} \; \forall g \in \Omega_{\text{G}} \tag{50}$$

$$Q_{\text{G},g}^{\min} \leq Q_{\text{G},g} \leq Q_{\text{G},g}^{\max} \; \forall g \in \Omega_{\text{G}} \tag{51}$$

Here, constraints (46)-(48) impose power flow of distribution lines. Constraint (49) imposes bounds on nodal voltages. Constraints (50)-(51) impose the upper/lower bound on generators output. $S_{i,j}^{\max}$ is maximum allowable capacity of distribution line (i,j). $U_j^{\min}$ and $U_j^{\max}$ are the minimum and maximum values of node voltage. $P_{\text{G},g}^{\min}$ and $P_{\text{G},g}^{\max}$ are the minimum and maximum values of active power of the generator. $Q_{\text{G},g}^{\min}$ and $Q_{\text{G},g}^{\max}$ are the minimum and maximum values of reactive power of the generator.

The above OPF-SOCR is a second-order cone programming problem and can be effectively solved using CPLEX or Mosek solvers.

III. DISTRIBUTED COORDINATED OPERATION METHOD FOR INTEGRATED TRANSPORTATION-POWER ENERGY SYSTEMS

In order to promote the coordinated operation of TNs and PDNs while ensuring data privacy between the two networks, the idea of ADMM is adopted to design a distributed coordinated operation method and solution algorithm for ITPES. This method aims to determine appropriate nodal marginal electricity prices to guide the dynamic wireless charging behavior of EVs, enabling them to make socially optimal driving and charging decisions and achieve optimal energy consumption.

A. METHOD OVERVIEW

The established TAP-ECD and OPF-SOCR are coupled through the load constraints of WCSs represented by (52):

$$\begin{aligned} P_{\text{Lc},s} &= \sum_{a=1}^{N_s} \sum_{w=1}^{N_{\Omega_{\text{QD}}}} \sum_{ke=1}^{N_{\Omega_{\text{KEV},w}}} H_{EV,ke,w} E_{a,ke,w} \;\; \forall s \in \Omega_{\text{WCS}} \\ P_{\text{Lc},s}^{\text{E}} &= P_{\text{Lc},s}^{\text{T}} \end{aligned} \tag{52}$$

Here, $P_{\text{Lc},s}^{\text{E}}$ and $P_{\text{Lc},s}^{\text{T}}$ represent the optimized charging loads obtained from the TN and the PDN, respectively.

Based on the ADMM [34], by introducing the Lagrange multiplier ρ_s, the coupling constraints (52) are relaxed, and an augmented Lagrangian function for ITPES is established, as shown in (53):

$$\begin{aligned} L(P_{\text{Lc},s}^{\text{T}}, P_{\text{Lc},s}^{\text{E}}, \rho) = {} & F_{\text{TAP}}(P_{\text{Lc},s}^{\text{T}}) + F_{\text{E}}(P_{\text{Lc},s}^{\text{E}}) \\ & + \sum_{s=1}^{N_{\Omega_{\text{WCS}}}} \rho_s (P_{\text{Lc},s}^{\text{T}} - P_{\text{Lc},s}^{\text{E}}) \\ & + \sum_{s=1}^{N_{\Omega_{\text{WCS}}}} \frac{b}{2} \left\| P_{\text{Lc},s}^{\text{T}} - P_{\text{Lc},s}^{\text{E}} \right\|_2^2 \end{aligned} \tag{53}$$

This augmented Lagrangian function can be decomposed into three subproblems, which are the $P_{\text{Lc},s}^{\text{T}}-update$ subproblem 1, $P_{\text{Lc},s}^{\text{E}}-update$ subproblem 2 and Lagrange multipliers updating subproblem 3. Specifically, the TAP-ECD is $P_{\text{Lc},s}^{\text{T}}-update$ subproblem 1, and the OPF-SOCR is $P_{\text{Lc},s}^{\text{E}}-update$ subproblem 2. The detailed model is provided below:

$$P_{\text{Lc},s}^{\text{T},k+1} \in \underset{P_{\text{Lc},s}^{\text{T}} \in \Omega_{\text{TAP}}}{\arg\min} \left\{ \begin{aligned} & F_{\text{TAP}} + \sum_{s=1}^{N_{\Omega_{\text{WCS}}}} \rho_s (P_{\text{Lc},s}^{\text{T}} - P_{\text{Lc},s}^{\text{E},k}) \\ & + \sum_{s=1}^{N_{\Omega_{\text{WCS}}}} \frac{b}{2} \left\| P_{\text{Lc},s}^{\text{T}} - P_{\text{Lc},s}^{\text{E},k} \right\|_2^2 \end{aligned} \right\} \tag{54}$$

$$P_{\mathrm{Lc},s}^{\mathrm{E},k+1} \in \underset{P_{\mathrm{Lc},s}^{\mathrm{E}} \in \Omega_{\mathrm{OPF}}}{\arg\min} \left\{ \begin{array}{l} F_{\mathrm{E}} + \sum_{s=1}^{N_{\Omega_{\mathrm{WCS}}}} \rho_s (P_{\mathrm{Lc},s}^{\mathrm{T},k+1} - P_{\mathrm{Lc},s}^{\mathrm{E}}) \\ + \sum_{s=1}^{N_{\Omega_{\mathrm{WCS}}}} \frac{b}{2} \left\| P_{\mathrm{Lc},s}^{\mathrm{T},k+1} - P_{\mathrm{Lc},s}^{\mathrm{E}} \right\|_2^2 \end{array} \right\} \tag{55}$$

$$\rho_s^{k+1} = \rho_s^k + b \left(P_{\mathrm{Lc},s}^{\mathrm{T},k+1} - P_{\mathrm{Lc},s}^{\mathrm{E},k+1} \right) \ \forall s \in \Omega_{\mathrm{WCS}} \tag{56}$$

Here, Ω_{TAP} is constraint set of the TAP-ECD in TN. Ω_{OPF} is constraint set of the OPF-SOCR in PDN.

B. SOLUTION ALGORITHM

The coordinated operation method for ITPES can be solved by addressing the $P_{\mathrm{Lc},s}^{\mathrm{T}} - update$ subproblem 1, $P_{\mathrm{Lc},s}^{\mathrm{E}} - update$ subproblem 2 and updating Lagrange multipliers. The iteration process terminates when the original and dual residuals, as indicated in equations (57) and (58), satisfy convergence conditions. At this point, the optimal nodal marginal electricity prices are obtained. Under these prices, the ITPES achieves its socially optimal operating state. The specific distributed coordinated operation algorithm for ITPES is outlined in TABLE 3.

$$\max \left\{ \left| P_{\mathrm{Lc},s}^{\mathrm{T},k+1} - P_{\mathrm{Lc},s}^{\mathrm{E},k+1} \right| \forall s \in \Omega_{\mathrm{WCS}} \right\} \tag{57}$$

$$\max \left\{ \left| P_{\mathrm{Lc},s}^{\mathrm{T},k+1} - P_{\mathrm{Lc},s}^{\mathrm{T},k} \right|, \left| P_{\mathrm{Lc},s}^{\mathrm{E},k+1} - P_{\mathrm{Lc},s}^{\mathrm{E},k} \right| \forall s \in \Omega_{\mathrm{WCS}} \right\} \tag{58}$$

The overall flowchart of the solution methodology (Algorithm 1 and 2) is summarized in Figure 1.

IV. CASE STUDIES

A. BASIC SETTING

A test system with an emblematical ring expressway TN [8] and an improved 11 kV radial PDN [35] is adopted to demonstrate effectiveness of the proposed model and algorithm. The topology of the TN and PDN and coupling relationships are illustrated in Figure 2.

The electrified TN is composed of twelve nodes, four types of roads and eight WCSs located on the inner and outer rings. The characteristics of the roads and WCSs are given in TABLE 4. The traffic demand $q_{\mathrm{GV},w}$ of GVs and potential initial charging demand $q_{\mathrm{EV},w}$ of EVs for eleven OD pairs are listed in TABLE 5. As for PDN, it consists of 119 buses, 118 distribution lines and three generation units. Generators G1-G3 share the same parameters: $a_g = 0.3\$/\mathrm{MW}^2\mathrm{h}$, $b_g = 150\$/\mathrm{MWh}$, and the capacity is 3 MW. The base value of power is set as 10MVA. The voltage boundary is $\sqrt{U_{\min,j}} = 0.85$ and $\sqrt{U_{\max,j}} = 1.05$. The voltage magnitude at the slack bus is $\sqrt{U_0} = 1.02$. The capacity of each distribution line is $S_{i,j}^{\max} = 1.6$ p.u. for all lines.

B. PERFORMANCE ANALYSIS OF THE ALGORITHMS

In this section, the effectiveness of Algorithm 1 and the convergence and complexity of Algorithm 2 are investigated.

TABLE 6 and 7 respectively present the effective travel path sets for GVs and EVs between each OD pair in TN when the coupled network achieves coordinated operation. It is clear that the proposed effective path generation model and solution Algorithm 1 have eliminated redundant paths not chosen by users and optimized the effective path sets available for both EVs and GVs between each OD pair. Additionally, the travel time, travel cost, and traffic flow for GVs (EVs) on those effective travel paths are also successfully calculated. Notably, when multiple effective paths exist between an OD pair (e.g., T3-T10, T4-T9, T4-T10, T4-T12 for GVs; T4-T9 for EVs), the travel costs for GVs or EVs on each path are equal, which consistent with mixed UE state (Equations (14)-(15)). These results

TABLE 3. Distributed coordinated operation algorithm for ITPES.

Algorithm 2: Distributed coordinated operation algorithm for ITPES

Input:

1: Road information and OD matrix for TN.

2: Distribution lines and load information for PDN.

Initialization:

3: Set the current iteration count $k = 1$.

4: Initialize the charging load $P_{\mathrm{Lc},s}^{\mathrm{E},k} = 0, \forall s \in \Omega_{\mathrm{WCS}}$ in $P_{\mathrm{Lc},s}^{\mathrm{E}} - update$ subproblem 2.

5: Initialize nodal marginal electricity prices $\lambda_a^k = 0, \forall a \in \Omega_{\mathrm{A}}$

6: Initialize Lagrange multipliers $\rho_s^k = 0, \forall s \in \Omega_{\mathrm{WCS}}$.

Iterative program:

7: For $k = 1 : K_{\max}$ do

8: **Solve Subproblem 1:** Utilize Algorithm 1 to solve $P_{\mathrm{Lc},s}^{\mathrm{T}} - update$ subproblem 1 to obtain the traffic flow distribution and charging load $P_{\mathrm{Lc},s}^{\mathrm{T},*}$ in TN. And then set $P_{\mathrm{Lc}}^{\mathrm{T},k+1} = P_{\mathrm{Lc}}^{\mathrm{T},*}, \forall s \in \Omega_{\mathrm{WCS}}$.

9: **Solve Subproblem 2:** Solve $P_{\mathrm{Lc},s}^{\mathrm{E}} - update$ subproblem 2 to acquire the power flow distribution, nodal marginal electricity prices $\lambda_a^*, \forall a \in \Omega_{\mathrm{A}}$, and charging load $P_{\mathrm{Lc},s}^{\mathrm{E},*}, \forall s \in \Omega_{\mathrm{WCS}}$ in PDN with the results from Step 8. And then set $\lambda_a^{k+1} = \lambda_a^*, \forall a \in \Omega_{\mathrm{A}}$, $P_{\mathrm{Lc}}^{\mathrm{E},k+1} = P_{\mathrm{Lc}}^{\mathrm{E},*}, \forall s \in \Omega_{\mathrm{WCS}}$.

10: **Convergence Check:** Calculate the original and dual residuals. If $\max \left\{ \left| P_{\mathrm{Lc},s}^{\mathrm{T},k+1} - P_{\mathrm{Lc},s}^{\mathrm{E},k+1} \right| \forall s \in \Omega_{\mathrm{WCS}} \right\} \le \varepsilon^{pri}$, $\max \left\{ \left| P_{\mathrm{Lc},s}^{\mathrm{T},k+1} - P_{\mathrm{Lc},s}^{\mathrm{T},k} \right|, \left| P_{\mathrm{Lc},s}^{\mathrm{E},k+1} - P_{\mathrm{Lc},s}^{\mathrm{E},k} \right| \forall s \in \Omega_{\mathrm{WCS}} \right\} \le \varepsilon^{dual}$, then the iteration process terminates, go to step 13. Otherwise, go to Step 11.

11: **Update Lagrange Multipliers:** Update Lagrange multipliers $\rho_s^{k+1}, \forall s \in \Omega_{\mathrm{WCS}}$ using (56) based on the charging load $P_{\mathrm{Lc}}^{\mathrm{T},k+1}$ and $P_{\mathrm{Lc}}^{\mathrm{E},k+1}$.

12: End for.

Output:

13: The optimal nodal marginal electricity prices.

14: The operating state of the ITPES.

TABLE 4. Characteristics of roads.

Road	I	II	III	IV
C_a (veh/h)	1000	1000	800	600
χ_a^0 (min)	10	7	10	5
d_a (km)	13.3	9.3	13.3	6.7
L_a (kW)	5	/	5	/

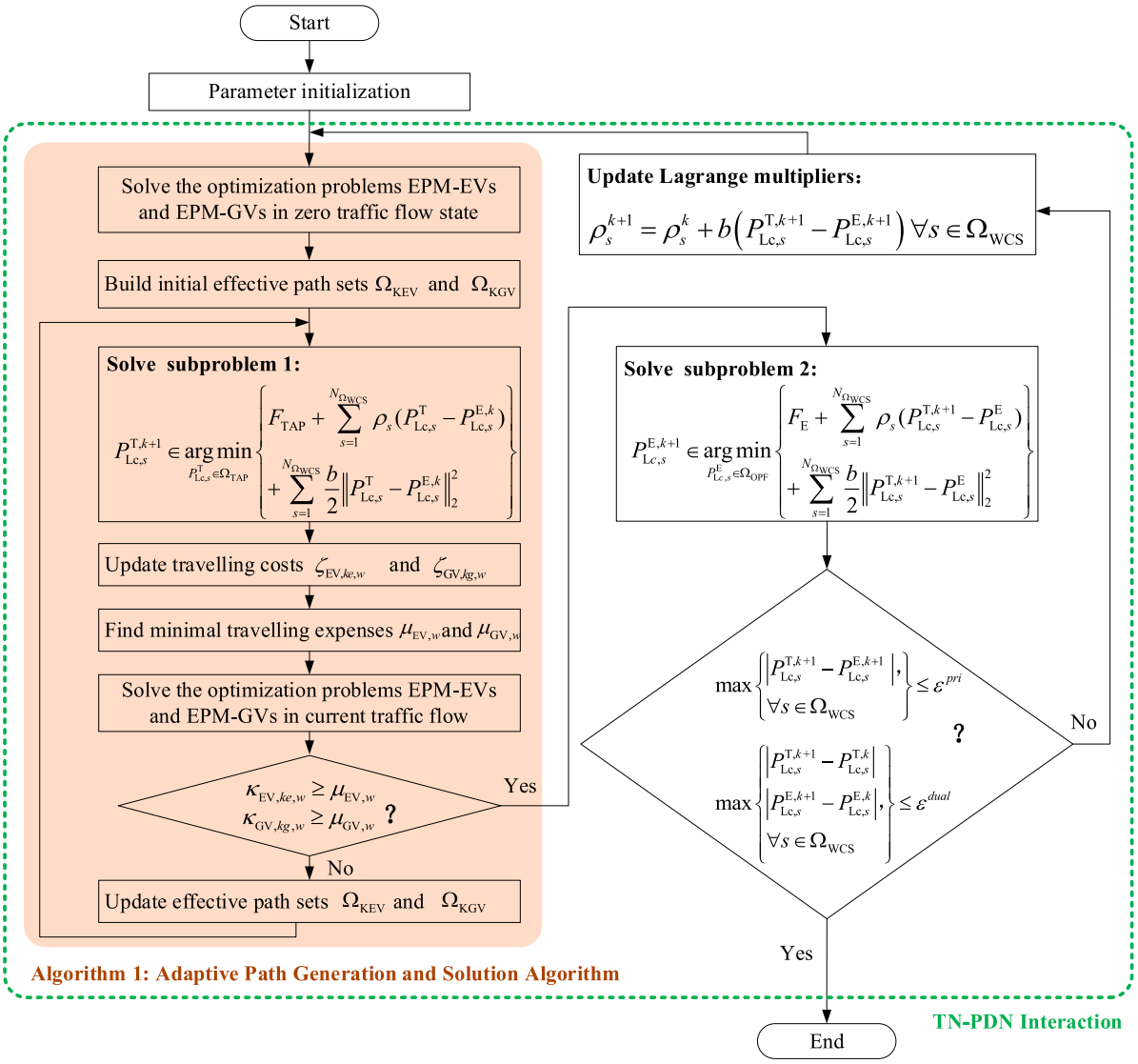

FIGURE 1. Flowchart of the solution methodology.

TABLE 5. OD pairs and their traffic demands (The penetration rate of EVs is 60%).

OD pairs	Form node	To node	$q_{GV,w}$ (veh/h)	$q_{EV,w}$ (veh/h)	Total demand (veh/h)
od1	T1	T6	230	90	320
od2	T1	T10	445	75	520
od3	T1	T11	325	75	400
od4	T1	T12	315	45	360
od5	T3	T6	250	90	340
od6	T3	T10	365	75	440
od7	T3	T11	295	105	400
od8	T3	T12	365	75	440
od9	T4	T9	375	105	480
od10	T4	T10	265	135	400
od11	T4	T12	325	75	400

largely validate the effectiveness of the proposed electrified TN model and adaptive path generation and solution Algorithm 1.

TABLE 6. Effective paths, travel time, travel cost and path traffic flow for GVs in each OD pair.

OD pairs	Form node	To node	Effective path	Time (min)	Travel cost ($)	Traffic flow (veh)
od1	T1	T6	T1-T2-T6	20.22	3.37	230.00
od2	T1	T10	T1-T2-T6-T10	30.80	5.13	445.00
od3	T1	T11	T1-T4-T8-T11	24.49	4.08	325.00
od4	T1	T12	T1-T2-T5-T9-T12	34.13	5.69	315.00
od5	T3	T6	T3-T4-T5-T6	24.29	4.05	250.00
od6	T3	T10	T3-T4-T5-T6-T10	34.88	5.81	20.18
			T3-T7-T8-T9-T10	34.88	5.81	344.82
od7	T3	T11	T3-T7-T11	20.72	3.45	295.00
od8	T3	T12	T3-T7-T11-T12	31.05	5.18	365.00
od9	T4	T9	T4-T8-T9	24.39	4.07	317.88
			T4-T5-T9	24.39	4.07	57.12
od10	T4	T10	T4-T5-T6-T10	29.80	4.97	264.87
			T4-T5-T9-T10	29.80	4.97	0.13
od11	T4	T12	T4-T8-T11-T12	29.69	4.95	259.90
			T4-T5-T9-T12	29.69	4.95	65.10

Figure 3 illustrates the convergence curve of the original and dual residuals in Algorithm 2. The primal residual

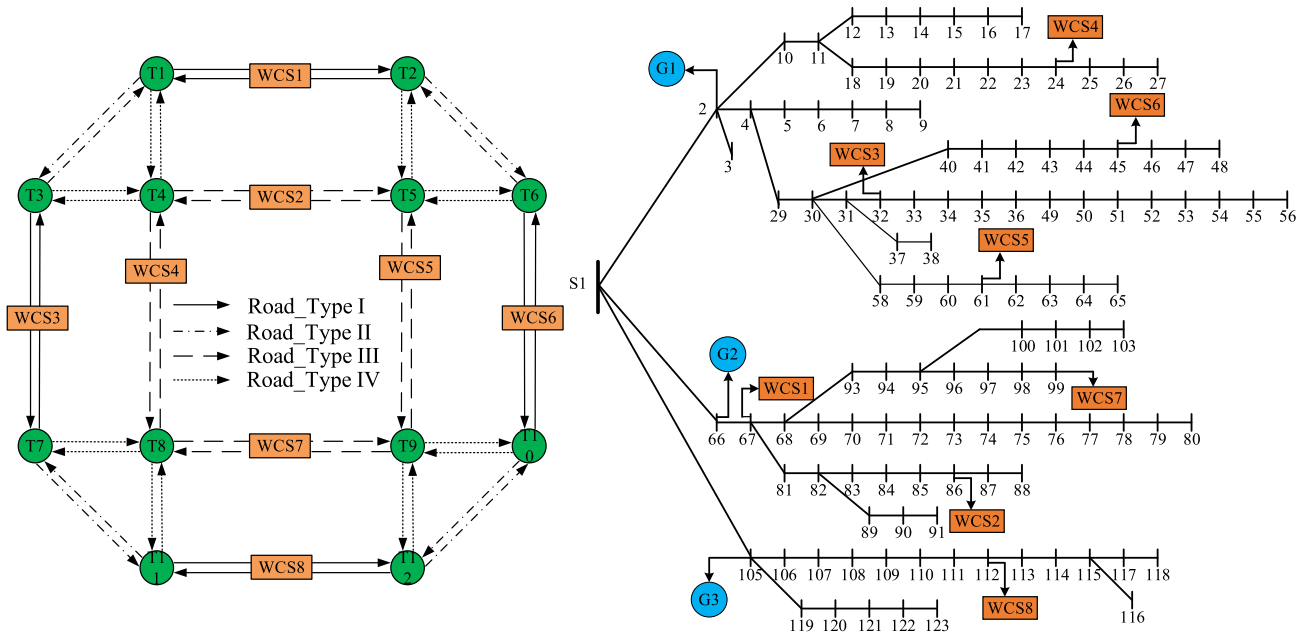

(a) Topology of the electrified TN

(b) Topology of the 119-bus PDN

FIGURE 2. The topology of the TN and PDN and coupling relationships.

TABLE 7. Effective paths, travel time, travel cost and path traffic flow for EVs in each OD pair.

OD pairs	Form node	To node	Effective path	Time (min)	Travel cost ($)	Traffic flow (veh)
od1	T1	T6	T1-T2-T6	20.22	3.99	78.35
od2	T1	T10	T1-T2-T6-T10	30.80	6.15	60.49
od3	T1	T11	T1-T4-T8-T11	24.49	4.85	63.37
od4	T1	T12	T1-T2-T5-T9-T12	34.13	6.82	35.45
od5	T3	T6	T3-T4-T5-T6	24.29	4.84	76.03
od6	T3	T10	T3-T7-T8-T9-T10	34.88	6.97	58.76
od7	T3	T11	T3-T7-T11	20.72	4.09	91.10
od8	T3	T12	T3-T7-T11-T12	31.05	6.22	60.30
od9	T4	T9	T4-T8-T9	24.39	4.84	11.03
			T4-T5-T9	24.39	4.84	77.68
od10	T4	T10	T4-T5-T9-T10	29.80	5.94	109.72
od11	T4	T12	T4-T5-T9-T12	29.69	5.92	60.99

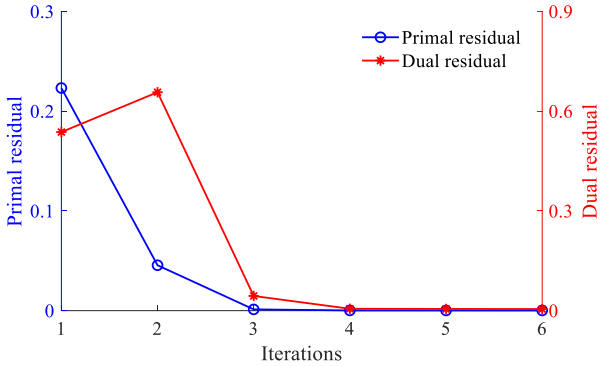

FIGURE 3. Primal and dual residual curves (The penetration rate of EVs is 60%).

reflects whether the coordinated operation of TN and PDN can be achieved. Meanwhile, dual residual is an important criterion to judge whether the distributed coordinated operation algorithm for ITPES achieves the optimal solution, and its variation trend can reflect the characteristics of the algorithm. It can be observed that after 6 iterations, both the original and dual residuals rapidly approach zero, satisfying the convergence conditions. It illustrates that the distributed coordinated operation method for ITPES can satisfy all kinds of constraints set by TN and PDN, and converge quickly to an optimum solution.

Now consider the computational complexity of the proposed two algorithms. The presented TAP-ECD ($P^{\mathrm{T}}_{\mathrm{Lc},s}$ – *update* subproblem 1) and OPF-SOCR ($P^{\mathrm{E}}_{\mathrm{Lc},s}$ – *update* subproblem 2) problems are strictly convex nonlinear programming problem and second-order cone programming problem respectively, which can be efficiently solved by optimization software solvers IPOPT and Mosek, respectively. Meanwhile, as the two problems are convex, the Algorithm 2 will be able to converge to optimal solution with reasonable computation time. The computational time under different penetration rates of EVs is shown in Figure 4. It can be seen that under different EVs penetration rates, the proposed model can be solved by the proposed two algorithms in a reasonable amount of time. The maximum number of iterations for the Algorithm 2 is 10. The total computing times are 238s to 634s under different penetration rates of EVs. Compared to day-ahead scheduling, and even to a 60-minute dispatch interval, the proposed algorithms are fast enough to support managers in promoting the coordinated operation of ITPES.

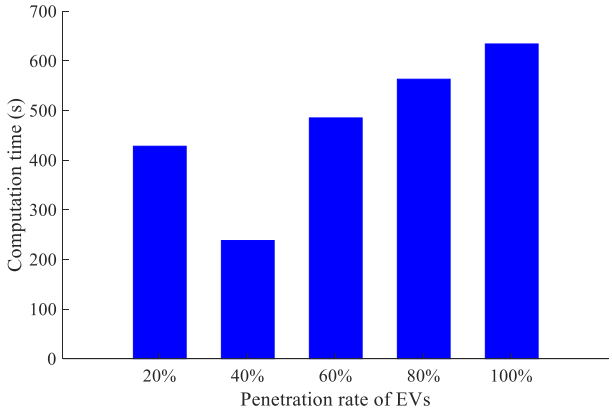

FIGURE 4. Computation time under different penetration rates of EVs.

C. RESULTS AND ANALYSIS OF THE PROPOSED MODEL

To analyze the effectiveness of the proposed model, two scenarios are intentionally designed and compared.

Scenario 1: Non-coordinated operation of the ITPES. There is no interaction be-tween the TN and PDN. All the electricity prices of WCSs are equal to each other, uniformly fixed at \$180/MWh, which will not affect the routing selection and charging decisions of EVs.

Scenario 2: Coordinated operation of the ITPES (proposed method).

1) COSTS ANALYSIS FOR THE INTEGRATED TRANSPORTATION-POWER ENERGY SYSTEMS

The costs analysis for the ITPES in both scenarios is presented in TABLE 8. Compared to Scenario 1, Scenario 2 exhibits a significant reduction in various costs, including electricity purchasing cost F_{sub} from the wholesale power market, production cost F_{G} of generators, total traffic delay cost F_T and charging cost F_{CH} for all of the EVs. The operation cost F_{E} of PDN reaches a minimum value of \$4265.63, and the total travelling cost ($F_{\text{T}} + F_{\text{CH}}$) of TN reaches a minimum value of \$18420.48 in Scenario 2. These reductions of 8.34% and 3.68% in costs compared to Scenario 1, respectively, demonstrate the superiority of achieving coordinated operation for ITPES.

TABLE 8. Costs of objective function in PDN and TN.

Scenarios	Electricity purchasing cost F_{sub} (\$)	Production cost of generators F_{G} (\$)	Total traffic delay cost F_T (\$)	Total charging cost F_{CH} (\$)
1	4006.86	646.95	17930.17	1194.88
2	3669.89	595.74	17736.78	683.70

TABLE 9 provides the travelling costs for EVs and GVs between each OD pairs in Scenario 2. It is observed that the travelling cost of EVs is slightly higher than that of GVs between each OD pair. This is due to the driving range limitations of EVs battery, which require additional recharging expenses for EVs to fulfill their travel plans, we do not include the refueling cost of GVs.

TABLE 9. Travel costs of EV and GV in each OD pair.

OD pairs	Form node	To node	Travel cost for GVs (\$)	Travel cost for EVs (\$)
od1	T1	T6	3.37	3.99
od2	T1	T10	5.13	6.15
od3	T1	T11	4.08	4.85
od4	T1	T12	5.69	6.82
od5	T3	T6	4.05	4.84
od6	T3	T10	5.81	6.97
od7	T3	T11	3.45	4.09
od8	T3	T12	5.18	6.22
od9	T4	T9	4.07	4.84
od10	T4	T10	4.97	5.94
od11	T4	T12	4.95	5.92

2) OPTIMIZATION RESULTS ANALYSIS OF TRANSPORTATION NETWORK

Figure 5 presents the actual charging demand $q_{\text{EV,real},w}$ after EVs response in both Scenarios. It is evident that the actual charging demand $q_{\text{EV,real},w}$ of each OD pair in both Scenario 1 and Scenario 2 is less than the initial charging demand $q_{\text{EV},w}$. Some EVs, influenced by traffic delay and charging costs, abandon their original travel and charging plans. It demonstrates that the TAP-ECD presented in Section II is able to reflect the elastic charging behavior of EVs to calculate the actual charging demand.

Furthermore, in Scenario 2, the actual charging demand $q_{\text{EV,real},w}$ for each OD pair is less than in Scenario 1, indicating that more EVs are abandoning their original travelling and charging plans. The primary reason lies in the coordinated operation mode, where the TN and PDN achieve coordinated interaction through node marginal electricity prices. Disparities in electricity pricing result in variations in charging costs. Consequently, the elastic response behavior of EVs is no longer solely influenced by traffic delay costs; instead, discrepancies in charging expenses encourage more users to give up travel and charging plans.

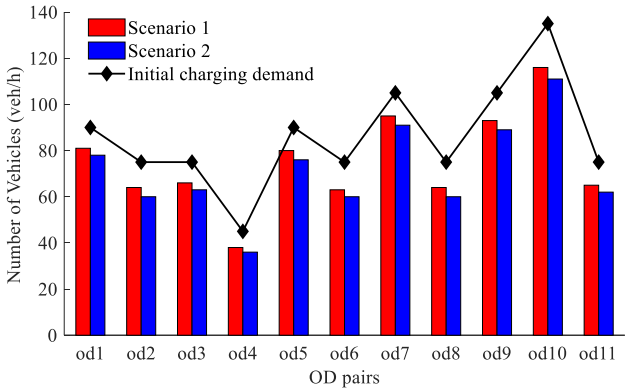

FIGURE 5. Changing demand of EVs in each OD pair.

Figure 6 displays the traffic flows distribution of EVs and GVs in each road of TN. It is observed that: (1) in both

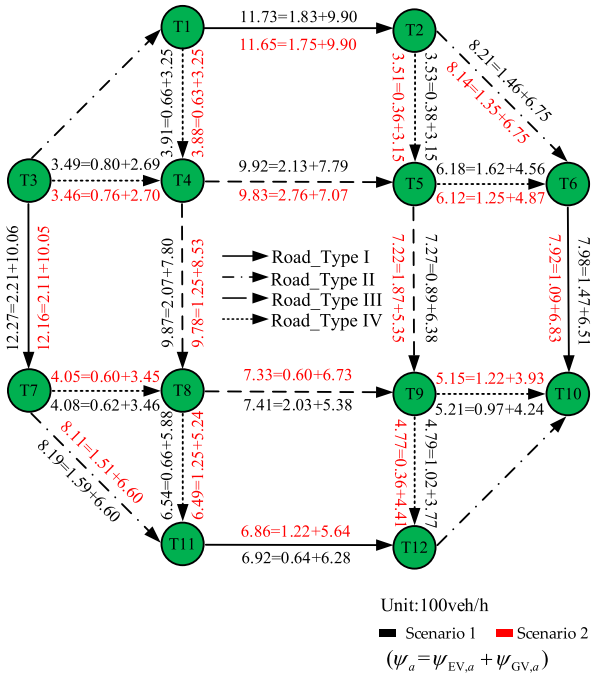

FIGURE 6. Traffic flows distribution in TN.

scenarios, most vehicles choose to travel on the inner and outer ring expressways of the TN, as they have higher road capacities and fewer traffic signals (indicated by smaller χ_a^0); (2) Compared to Scenario 1, the total traffic flow in each road of Scenario 2 has decreased, indicating that regulating the elastic charging behavior of EVs through nodal marginal electricity prices is effective in alleviating traffic congestion.

To further illustrate SOC of EVs at each road node and charging electricity quantity $E_{a,ke,w}$ at WCS along the effective travel path, we conduct a detailed analysis using the effective travel paths T1-T2-T6-T10, T3-T7-T8-T9-T10, and T4-T5-T9 as examples. Attentively, the minimum threshold m for the SOC of EVs is set at 10% of the battery capacity, the initial SOC of EVs is uniformly set to 30% of the battery capacity, and the final SOC must also be maintained at 30% of the battery capacity or higher by the trip's end.

Figure 7 shows SOC of EVs at each road node and charging electricity quantity at WCS along the effective travel path in two Scenarios. It is can be seen that in both Scenarios, all the constraints on SOC of EVs in EPM-EVs can be satisfied. In addition, the charging electricity quantity $E_{a,ke,w}$ of EVs at each WCS along the travel route reached maximum limit of 5kWh in Scenario 1. In contrast, in Scenario 2, the charging electricity quantity $E_{a,ke,w}$ of EVs at each WCS along the effective travel route was regulated to ensure that it can only meet the minimum requirement, maintaining a SOC 30% of the battery capacity by the trip's end. These results demonstrate that the proposed EPM-EVs effectively describes SOC of EVs at each road node across different travel paths. It also enables the regulation and optimization of EV charging electricity quantities $E_{a,ke,w}$ at WCS along the travel route.

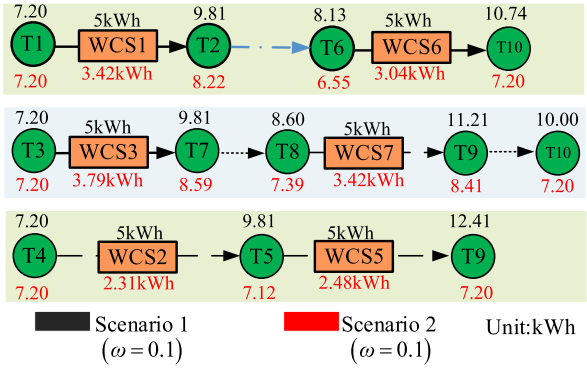

FIGURE 7. SOC of EVs at each road node and charging electricity quantity for EVs at WCS along the effective travel path.

In Scenario 2, we further investigate how the recharging willingness of EV drivers affects the charging electricity quantities $E_{a,ke,w}$ at WCS along the travel route. The symbol ω in Formula (20) represents willingness of EV drivers to fully recharge the battery, it is set to three different parameter values, such as 0.1,0.5,1. Relevant results are displayed in Figure 7 and Figure 8, from which there are the following findings: Among the three effective paths listed, an increase in EV drivers' willingness to recharge leads to a higher charging electricity quantities $E_{a,ke,w}$ at each WCSs along the travel route, indicating the proposed utility function model can describe the charging willingness of EV drivers. Namely, the stronger the willingness of EV drivers to fully recharge the battery, the larger the charging electricity quantities $E_{a,ke,w}$ obtained through optimization.

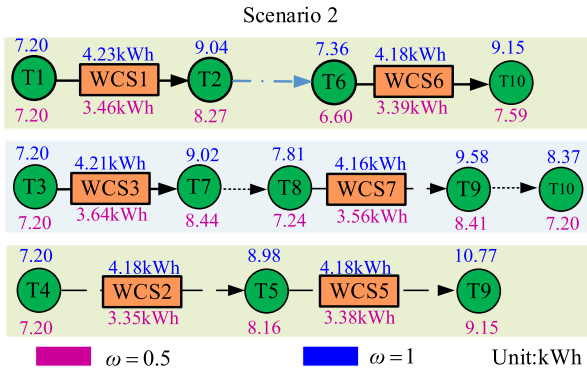

FIGURE 8. SOC of EVs at each road node and charging electricity quantity for EVs at WCS along the effective travel path in Scenario 2 (ω = 0.5 and ω = 1).

3) OPTIMIZATION RESULTS ANALYSIS OF POWER DISTRIBUTION NETWORK

The optimization results of purchasing power from the wholesale power market or main grid, scheduling plans of generators, and bus voltage in PDN are presented in TABLE 10 and Figure 9. It can be found that all security constraints in PDN are maintained in both Scenarios, however, Scenario 1 shows higher purchasing power from the wholesale market and greater generator active power output compared to Scenario 2. Additionally, the voltage magnitudes

at some buses connected to WCSs in Scenario 1 are lower than those Scenario 2. These results indicate that the coordinated operation of ITPES can reduce the charging demand of EVs, improve the spatial distribution of charging loads, thus the active power output of the PDN is reduced effectively, enhancing voltage quality.

TABLE 10. Purchasing power from main grid and dispatching of generators.

Line	Active power (MW)		Reactive power (MW)	
	Scenario 1	Scenario 2	Scenario 1	Scenario 2
1-2	12.31	11.23	7.51	7.43
1-66	9.89	8.85	4.67	4.59
1-105	4.51	4.39	3.16	3.16
Node	Active power (MW)		Reactive power (MW)	
	Scenario 1	Scenario 2	Scenario 1	Scenario 2
2	1.86	1.69	1.00	1.00
66	1.21	1.07	1.00	1.00
115	1.24	1.20	1.00	1.00

TABLE 11 summarizes optimization results of node marginal electricity prices and charging load. From TABLE 11, it is evident that compared to Scenario 1, the WCSs in Scenario 2 exhibit lower nodal marginal electricity prices, and the difference between the highest and lowest prices is smaller. Because, in the coordinated operation mode, nodal marginal electricity prices influenced the routing selection and charging decisions of EVs, thereby affecting the charging loads of WCSs. The variation in charging loads, in turn, affects the operating state of PDN, and consequently alters the marginal electricity price at nodes. Through this coordinated interaction between the TN and PDN, a coordinated equilibrium state is achieved, resulting in relatively uniform nodal marginal electricity prices.

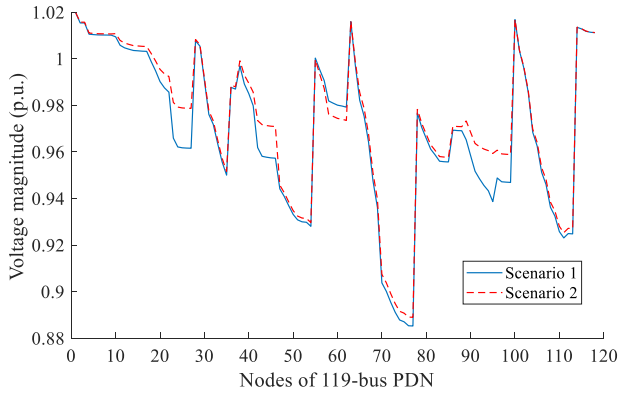

FIGURE 9. Bus voltage magnitudes of PDN.

4) SENSITIVITY ANALYSIS OF ELASTICITY COEFFICIENT

Elasticity coefficient θ is a very important parameter in TAP-ECD, and the change of this parameter will determine whether the proposed detailed electrified TN model, distributed coordinated operation method and corresponding solution algorithm have a promising application in the real world. Therefore, we investigate the impacts of the elasticity coefficient from different aspects, including operation cost F_{E}

TABLE 11. Node marginal electricity price and charging load of DWCs.

WCS	Node marginal electricity prices ($/MWh)		Charging loads (MW)	
	Scenario 1	Scenario 2	Scenario 1	Scenario 2
1	154.05	153.59	0.92	0.66
2	165.00	164.30	1.07	1.03
3	157.71	157.20	1.11	0.80
4	164.85	159.01	1.04	0.34
5	159.04	160.94	0.45	0.83
6	165.77	161.04	0.73	0.18
7	172.33	164.71	1.02	0.23
8	168.44	167.61	0.32	0.18

of PDN, total travelling cost ($F_{\mathrm{T}} + F_{\mathrm{CH}}$) of TN, and charging demand of each OD pair. The corresponding simulation results are provided in Figure 10-11.

From Figure 10 and Figure 11, it can be seen that as the elasticity coefficient increases, both the operational costs for PDN and travelling costs for TN decrease. The charging demand of each OD pair also declines, with more EVs abandoning their initial travel and charging plans. Additionally, the gap between the charging demands for each OD pair narrows, leading to a more uniform travelling distribution of charging demand across the TN with a larger elasticity coefficient.

These phenomena occur because, with larger elasticity coefficients, the willingness of EVs to travel and recharge diminishes, while their sensitivity (the degree of elastic response) to travelling costs increases. The proposed model and method for ITPES more efficiently regulates the travel and recharge plans of EVs. As a result, more EVs abandon their original travelling and recharging plans or choose other means of transportation, reducing the overall charging demand. The reduction in charging demand has lowered the overall charging load, thereby reducing both the total operating cost of PDN and the total travelling cost of TN.

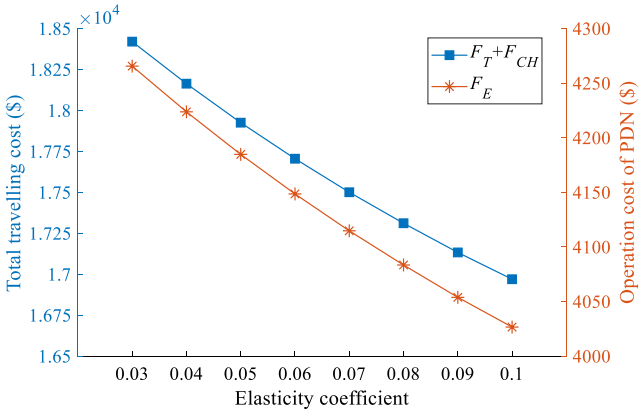

FIGURE 10. Operation cost of PDN and total travelling cost of TN under different elasticity coefficient.

The above results demonstrate that the proposed TAP-ECD model effectively describes elastic behavior of EV drivers to travelling costs, and the elasticity coefficient has a certain influence on the proposed model and method. In practical applications, the dispatching operator should set the elasticity

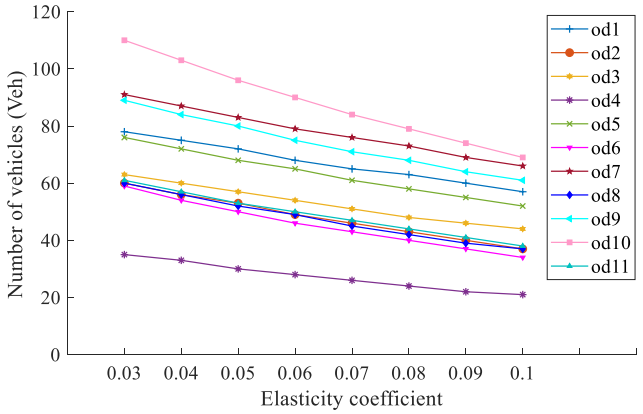

FIGURE 11. Charging demands under different elasticity coefficient.

coefficient based on the recharging willingness of EVs and the load level of the PDN to achieve flexible control of the elastic charging demand of EVs.

5) IMPACT ANALYSIS OF EVS PENETRATION

In the process of electrification transformation of TN, the penetration rate of EVs will affect the nodal marginal electricity prices in PDN. The adjustment of node marginal electricity prices will affect the routing selection and charging decisions of EVs, changing their charging location and charging electricity quantity, and thus affecting the spatio-temporal distribution of charging load. Therefore, in this section, the impacts of EVs market penetration rate on the coordinated operation of ITPES are investigated.

The spatial distribution of dynamic wireless charging load is illustrated in Figure 12, depicting the scenario where the total number of vehicles in the TN remains constant while gradually increasing the penetration rate of EVs. It is observed that the overall scale of charging loads continues to increase with the rising penetration rate of EVs, and its spatial distribution undergoes changes. When the penetration rate is below 60%, the charging loads at each WCS show a linear growth trend. However, when the penetration rate surpasses 60%, the charging loads exhibit nonlinear changes. The reason for this phenomenon is that the charging demand from EVs is relatively low and the power flows in the PDN will not change much. The routing selection and charging decisions of EVs remain consistent with the initial state. Therefore, the charging loads at each WCS grow linearly. As the penetration rate of EVs increases, the charging demand grows, causing significant changes in the power flow of the PDN. This affects the trend of nodal marginal price changes (as shown in Figure 13). Influenced by mileage limitation and travelling cost, some EVs alter their routing selection and charging decisions, resulting in nonlinear changes in charging loads.

Moreover, the penetration rate of EVs also influences the total operation cost F_{E} of PDN and total traffic delay cost F_T of TN. As presented in Figure 14, the total operation cost F_{E} of PDN shows an upward trend with the increase of EVs market penetration, while the total travel delay cost F_T of the

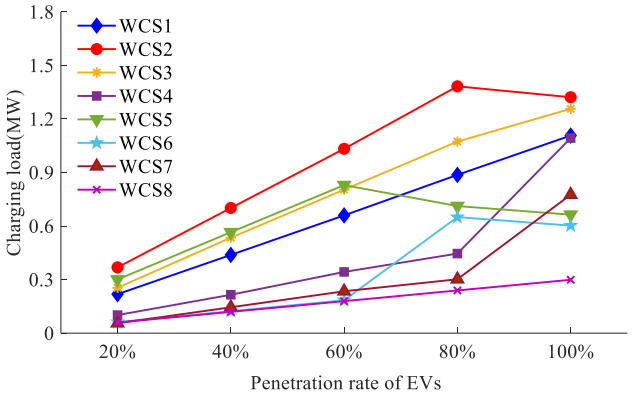

FIGURE 12. Relationship between charging loads and penetration rate of EVs.

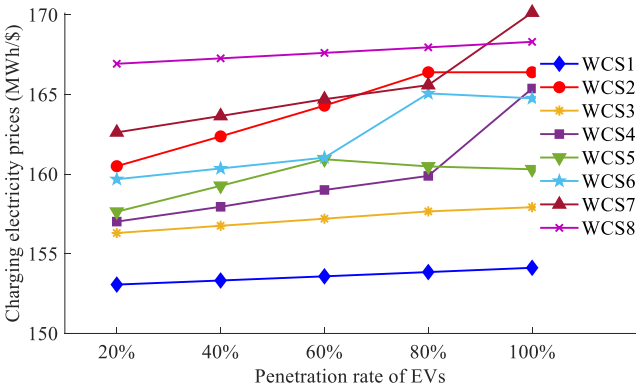

FIGURE 13. Relationship between charging electricity prices and penetration rate of EVs.

TN exhibits a decreasing trend. The main reason is that the rising market penetration of EVs increases the overall scale of charging loads, leading to a higher total operation cost F_{E} of PDN. As GVs decrease and EVs with elastic demand increase, more vehicles can be regulated by nodal marginal electricity prices. Consequently, traffic congestion is further alleviated, leading to a gradual reduction in total travel delay costs.

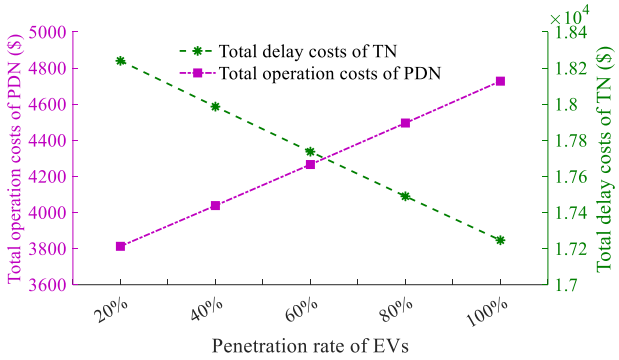

FIGURE 14. Relationship between costs and penetration rate of EVs.

V. CONCLUSION

To promote the coordinated operation of TNs and PDNs, this paper proposes a modeling framework and corresponding solution algorithms considering the elastic charging behavior

and mileage limitation of EVs. The main conclusions drawn from simulation results are as follows:

1) The TAP-ECD and the effective path generation models established in the TN can compute the actual charging demand of EVs and traffic flow distribution through the adaptive path generation and solution algorithm.
2) The distributed coordinated operation method and solution algorithm based on the ADMM for ITPES can determine appropriate nodal marginal electricity prices. These prices guide the dynamic wireless charging behavior of EVs, enabling them to make socially optimal driving and charging decisions and achieve optimal energy consumption.
3) The penetration rate of EVs significantly influences the overall scale and spatial distribution of dynamic wireless charging loads. Simultaneously, with an increase in the penetration rate, the total operation cost of PDN exhibits an increasing trend, while the total travel delay cost in TN shows a decreasing trend.

The effectiveness of the proposed modeling framework and corresponding solution algorithms has been demonstrated through case studies and comparisons, however, our current approach does not account for certain uncertainties [36], [37], such as the variable power output from renewable energy sources, traffic demand prediction errors, and the random driving behavior of traffic users. As an immediate next step, we plan to incorporate these uncertainties, integrate renewable energy generation into the ITPES, and expand our modeling framework and solution algorithms to further enhance the coordinated operation of TN and PDN.

REFERENCES

[1] Y. Shang and S. Li, "FedPT-V2G: Security enhanced federated transformer learning for real-time V2G dispatch with non-IID data," *Appl. Energy*, vol. 358, Mar. 2024, Art. no. 122626, doi: 10.1016/j.apenergy.2024.122626.

[2] Int. Energy Agency. (2023). *Global EV Outlook 2023*. [Online]. Available: https://www.iea.org/reports/global-ev-outlook-2023

[3] J. Xiong, K. Zhang, Y. Guo, and W. Su, "Investigate the impacts of PEV charging facilities on integrated electric distribution system and electrified transportation system," *IEEE Trans. Transport. Electrific.*, vol. 1, no. 2, pp. 178–187, Aug. 2015, doi: 10.1109/TTE.2015.2443798.

[4] W. Wei, D. WU, Q. WU, M. Shafie-Khah, and J. P. S. Catalão, "Interdependence between transportation system and power distribution system: A comprehensive review on models and applications," *J. Mod. Power Syst. Clean Energy*, vol. 7, no. 3, pp. 433–448, May 2019, doi: 10.1007/s40565-019-0516-7.

[5] Y. Sun, P. Zhao, L. Wang, and S. M. Malik, "Spatial and temporal modelling of coupled power and transportation systems: A comprehensive review," *Energy Convers. Econ.*, vol. 2, no. 2, pp. 55–66, Jun. 2021, doi: 10.1049/enc2.12034.

[6] M. Alizadeh, H.-T. Wai, M. Chowdhury, A. Goldsmith, A. Scaglione, and T. Javidi, "Optimal pricing to manage electric vehicles in coupled power and transportation networks," *IEEE Trans. Control Netw. Syst.*, vol. 4, no. 4, pp. 863–875, Dec. 2017, doi: 10.1109/TCNS.2016.2590259.

[7] F. He, Y. Yin, J. Wang, and Y. Yang, "Sustainability SI: Optimal prices of electricity at public charging stations for plug-in electric vehicles," *Netw. Spatial Econ.*, vol. 16, no. 1, pp. 131–154, Mar. 2016, doi: 10.1007/s11067-013-9212-8.

[8] W. Wei, L. Wu, J. Wang, and S. Mei, "Network equilibrium of coupled transportation and power distribution systems," *IEEE Trans. Smart Grid*, vol. 9, no. 6, pp. 6764–6779, Nov. 2018, doi: 10.1109/TSG.2017.2723016.

[9] L. Geng, Z. Lu, L. He, J. Zhang, X. Li, and X. Guo, "Smart charging management system for electric vehicles in coupled transportation and power distribution systems," *Energy*, vol. 189, Dec. 2019, Art. no. 116275, doi: 10.1016/j.energy.2019.116275.

[10] S. Xie, Q. Wu, N. D. Hatziargyriou, M. Zhang, Y. Zhang, and Y. Xu, "Collaborative pricing in a power-transportation coupled network: A variational inequality approach," *IEEE Trans. Power Syst.*, vol. 38, no. 1, pp. 783–795, Jan. 2023, doi: 10.1109/TPWRS.2022.3162861.

[11] J. Li, X. Xu, Z. Yan, H. Wang, M. Shahidehpour, and Y. Chen, "Coordinated optimization of emergency response resources in transportation-power distribution networks under extreme events," *IEEE Trans. Smart Grid*, vol. 14, no. 6, pp. 4607–4620, Nov. 2023, doi: 10.1109/TSG.2023.3257040.

[12] C. Shao, K. Li, T. Qian, M. Shahidehpour, and X. Wang, "Generalized user equilibrium for coordination of coupled power-transportation network," *IEEE Trans. Smart Grid*, vol. 14, no. 3, pp. 2140–2151, May 2023, doi: 10.1109/TSG.2022.3206511.

[13] S. Lv, S. Chen, Z. Wei, and G. Sun, "Security-constrained optimal traffic-power flow with adaptive convex relaxation and contingency filtering," *IEEE Trans. Transport. Electrific.*, vol. 9, no. 1, pp. 1605–1617, Mar. 2023, doi: 10.1109/TTE.2022.3175499.

[14] S. Liu, D. Z. W. Wang, Q. Tian, and Y. H. Lin, "Optimal configuration of dynamic wireless charging facilities considering electric vehicle battery capacity," *Transp. Res. E, Logistics Transp. Rev.*, vol. 181, Jan. 2024, Art. no. 103376, doi: 10.1016/j.tre.2023.103376.

[15] C. Li, X. Dong, L. M. Cipcigan, M. A. Haddad, M. Sun, J. Liang, and W. Ming, "Economic viability of dynamic wireless charging technology for private EVs," *IEEE Trans. Transport. Electrific.*, vol. 9, no. 1, pp. 1845–1856, Mar. 2023, doi: 10.1109/TTE.2022.3163823.

[16] F. He, Y. Yin, and J. Zhou, "Integrated pricing of roads and electricity enabled by wireless power transfer," *Transp. Res. C, Emerg. Technol.*, vol. 34, pp. 1–15, Sep. 2013, doi: 10.1016/j.trc.2013.05.005.

[17] S. D. Manshadi, M. E. Khodayar, K. Abdelghany, and H. Üster, "Wireless charging of electric vehicles in electricity and transportation networks," *IEEE Trans. Smart Grid*, vol. 9, no. 5, pp. 4503–4512, Sep. 2018, doi: 10.1109/TSG.2017.2661826.

[18] W. Wei, S. Mei, L. Wu, M. Shahidehpour, and Y. Fang, "Optimal traffic-power flow in urban electrified transportation networks," *IEEE Trans. Smart Grid*, vol. 8, no. 1, pp. 84–95, Jan. 2017, doi: 10.1109/TSG.2016.2612239.

[19] S. Lv, Z. Wei, G. Sun, S. Chen, and H. Zang, "Optimal power and semi-dynamic traffic flow in urban electrified transportation networks," *IEEE Trans. Smart Grid*, vol. 11, no. 3, pp. 1854–1865, May 2020, doi: 10.1109/TSG.2019.2943912.

[20] S. Lv, Z. Wei, S. Chen, G. Sun, and D. Wang, "Integrated demand response for congestion alleviation in coupled power and transportation networks," *Appl. Energy*, vol. 283, Feb. 2021, Art. no. 116206, doi: 10.1016/j.apenergy.2020.116206.

[21] J. C. Liu, H. Y. Zhang, A. Y. Liu, and S. Q. Cao, "Operation mechanism and co-optimization for electrified transportation-distribution networks with dynamic wireless charging," *Autom. Electr. Power Syst.*, vol. 46, no. 12, pp. 107–118, 2022, doi: 10.7500/AEPS20211122008.

[22] W. Wei, S. Mei, L. Wu, J. Wang, and Y. Fang, "Robust operation of distribution networks coupled with urban transportation infrastructures," *IEEE Trans. Power Syst.*, vol. 32, no. 3, pp. 2118–2130, May 2017, doi: 10.1109/TPWRS.2016.2595523.

[23] L. Geng, Z. Lu, X. Guo, J. Zhang, X. Li, and L. He, "Coordinated operation of coupled transportation and power distribution systems considering stochastic routing behaviour of electric vehicles and prediction error of travel demand," *IET Gener., Transmiss. Distrib.*, vol. 15, no. 14, pp. 2112–2126, Jul. 2021, doi: 10.1049/gtd2.12161.

[24] Y. Sheffy, *Urban Transportation Networks: Equilibrium Analysis With Mathematical Programming Methods* (Traffic Engineering Control). Upper Saddle River, NJ, USA: Prentice-Hall, 2112.

[25] N. H. Gartner, "Optimal traffic assignment with elastic demands: A review Part II. Algorithmic approaches," *Transp. Sci.*, vol. 14, no. 2, pp. 192–208, May 1980, doi: 10.1287/trsc.14.2.192.

[26] *Traffic Assignment Manual*, Bur. Public Roads, U.S. Dept. Commerce, Washington, DC, USA, 1964.

[27] W. Li, M. Jiang, Y. Chen, and M. C. Lin, "Estimating urban traffic states using iterative refinement and Wardrop equilibria," *IET Intell. Transp. Syst.*, vol. 12, no. 8, pp. 875–883, Oct. 2018, doi: 10.1049/iet-its.2018.0007.

[28] N. Jiang and C. Xie, "Computing and analyzing mixed equilibrium network flows with gasoline and electric vehicles," *Comput.-Aided Civil Infrastruct. Eng.*, vol. 29, no. 8, pp. 626–641, Sep. 2014, doi: 10.1111/mice.12082.
[29] C. Fisk, "Some developments in equilibrium traffic assignment," *Transp. Res. B, Methodol.*, vol. 14, no. 3, pp. 243–255, Sep. 1980.
[30] A.-H. Mohsenian-Rad, V. W. S. Wong, J. Jatskevich, R. Schober, and A. Leon-Garcia, "Autonomous demand-side management based on game-theoretic energy consumption scheduling for the future smart grid," *IEEE Trans. Smart Grid*, vol. 1, no. 3, pp. 320–331, Dec. 2010, doi: 10.1109/TSG.2010.2089069.
[31] L. Gan, N. Li, U. Topcu, and S. H. Low, "Exact convex relaxation of optimal power flow in radial networks," *IEEE Trans. Autom. Control*, vol. 60, no. 1, pp. 72–87, Jan. 2015, doi: 10.1109/TAC.2014.2332712.
[32] M. Farivar and S. H. Low, "Branch flow model: Relaxations and convexification—Part II," *IEEE Trans. Power Syst.*, vol. 28, no. 3, pp. 2565–2572, Aug. 2013, doi: 10.1109/TPWRS.2013.2255318.
[33] S. Huang, Q. Wu, J. Wang, and H. Zhao, "A sufficient condition on convex relaxation of AC optimal power flow in distribution networks," *IEEE Trans. Power Syst.*, vol. 32, no. 2, pp. 1359–1368, Mar. 2017, doi: 10.1109/TPWRS.2016.2574805.
[34] S. Boyd, "Distributed optimization and statistical learning via the alternating direction method of multipliers," *Found. Trends Mach. Learn.*, vol. 3, no. 1, pp. 1–122, 2010, doi: 10.1561/2200000016.
[35] D. Zhang, Z. Fu, and L. Zhang, "An improved TS algorithm for loss-minimum reconfiguration in large-scale distribution systems," *Electr. Power Syst. Res.*, vol. 77, nos. 5–6, pp. 685–694, Apr. 2007, doi: 10.1016/j.epsr.2006.06.005.
[36] Z. Li, L. Wu, Y. Xu, and X. Zheng, "Stochastic-weighted robust optimization based bilayer operation of a multi-energy building microgrid considering practical thermal loads and battery degradation," *IEEE Trans. Sustain. Energy*, vol. 13, no. 2, pp. 668–682, Apr. 2022, doi: 10.1109/TSTE.2021.3126776.
[37] S. Lv, S. Chen, Z. N. Wei, G. Q. Sun, and H. X. Zhang, "Review of modeling, solution methodology and application for coordinated operation of power and transportation systems," *Autom. Electr. Power Syst.*, to be published. [Online]. Available: https://link.cnki.net/urlid/32.1180.tp.20240702.1349.004

LIJUN GENG received the B.S. degree in electrical engineering and automation and the Ph.D. degree in power system and automation from Yanshan University, China, in 2015 and 2021, respectively. Since 2021, she has been a Lecturer with the Mechanical and Electrical Engineering College, Hebei Normal University of Science and Technology, Qinhuangdao, China. Her research interests include applied optimization and energy economics, coupled transportation, and power distribution systems.

CHENGXIA SUN received the B.S. degree in electrical engineering and automation and the Ph.D. degree in control science and engineering from Yanshan University, China, in 2015 and 2021, respectively. Since 2021, she has been a Lecturer with the Mechanical and Electrical Engineering College, Hebei Normal University of Science and Technology, Qinhuangdao, China. Her research interests include mechanisms for neural oscillation, modulation of neural oscillation, control theory, and complex network theory.

DONGDONG SONG was born in Qinhuangdao, Hebei, China, in 1981. He received the B.Sc. and M.S. degrees in electrical engineering from Hebei Agricultural University, Baoding, China, in 2005 and 2008, respectively, and the Ph.D. degree in agricultural electrification and automation from China Agriculture University, Beijing, China. Since 2008, he has been a Lecturer with the Mechanical and Electrical Engineering College, Hebei Normal University of Science and Technology, Qinhuangdao. His research interests include new energy power generation, intelligent monitoring of electrical equipment, and digital signal processing.

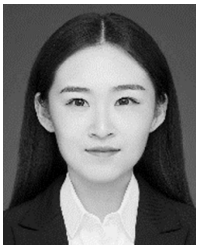

SHUANGHAN YANG received the master's degree in electrical engineering from Yanshan University, China, in 2021. She began to work with the Mechanical and Electrical Engineering College, Hebei Normal University of Science and Technology, China, in 2021. Her research interests include power converters, energy management, and power routing.

YUQUAN MA was born in January 1971. He received the bachelor's degree in electric machines from Xi'an Jiaotong University, in July 1993, and the master's degree in high voltage and insulation technology from Hebei University of Technology, in June 2009. Since 2002, he has been a Professor with the Mechanical and Electrical Engineering College, Hebei Normal University of Science and Technology, China. His research interest includes electrical control engineering and has presided over a technological innovation project, a DCS-based hardware-in-the-loop simulation system for the safe operation of styrene plants, supported by medium-sized scientific and technological enterprises in Hebei.

ZHIGANG LU was born in China, in 1961. He received the Ph.D. degree in electrical engineering from North China Electric Power University, in 1998. He is currently a Professor with the Key Laboratory of Power Electronics for Energy Conservation and Motor Drive, Yanshan University. His research interests include the economic operation of power systems, integrated energy systems, and emergency repair of power system faults. He is a member of the Chinese Society for Electrical Engineering and China Electrotechnical Society.